University of Zurich UZH

Department of Geography

Soil Dating and Redistribution in the Zofinsky Primeval Forest (Czech Republic)

GEO 511 Master's Thesis

Author

Teresa Steinert

12-708-335

Supervised by

Prof. Dr., Markus Egli

Dr., Samuel Abiven

Prof., Pavel Samonil — Department of Forest Ecology, Dendrology, Faculty of Forestry and Wood Sciences, Mendel University in Brno

pavel.samonil@vukoz.cz

Faculty representative

Prof. Dr., Markus Egli

14.07.2018

Department of Geography, University of Zurich

Summary

Tree uprooting is a worldwide phenomenon of intense bioturbation. It affects soil horizonation and interrupts the general slow but progressive evolution of soils. Several approaches were chosen to achieve knowledge about long- and short-term soil erosion. To relate such values in a better context, surface age and thus the age of the soils were gained. They were conducted in the Zofinsky primeval forest in the Czech Republic. This forest is strongly affected by tree uprootings. It is not disturbed by human impact due to strict protection since 1838.

With surface exposure dating using cosmogenic ^{10}Be, the soil surface and the outcrop of boulders can be detected. The soil in Zofinsky forest is roughly between 23 to 210 ka old. It corresponds mostly with the late Pleistocene. The tor can also be dated in the late Pleistocene. The surface lowering of the tor indicates a long-term erosion rate of 0.3 t/ha/year. In the Pleistocene glacial and interglacial periods alternated. The cold and dry climate had changed towards warmer and wetter conditions. The tundra-like vegetation cover changed slowly to boreal forest. We could date our boulders that were uplifted during tree uprootings in the late Holocene.

The hypothesis of undisturbed soil profiles could not be verified for one soil profile. It showed an unexpected distribution with depth indicating an old tree uprooting. Measured soil properties could not support recent soil disturbances. They showed typical distributions for the present soil type.

For short-term erosion rates the upper soil layer of the Zofinsky forest was analysed on changes of the radionuclide plutonium and the aggregate stability. The results provide information about the soil erosion for the current time and for the last half-century. It shows that the aggregates are stable to very stable. The short-term erosion rates based on changes of the plutonium shows higher erosion than the long-term rates. One exception shows deposition instead of erosion. The stable carbon isotope supports the results by giving qualitative information as an indicator of soil erosion.

Our findings enable us to reconstruct the soil development in the Zofinsky forest. The results provide insights into the effect of tree uprooting on soil development. More samples were already taken this summer. They will help to complete the findings in this thesis.

Table of Contents

Figures

Tables

1.   Introduction

Tree uprooting (TUR) is a worldwide phenomenon of intense bioturbation (Figure 1). It interrupts the slow but progressive soil evolution. Tree uprooting mainly affects soil horizonation, as it mixes materials that were originally stratified (Samonil et al., 2015). In temperate, beech-dominated European forest 1/3 of all trees die because of tree uprooting. The Zofinsky Primeval forest (Zofin forest) is also strongly influenced by tree uprooting. Tree uprooting microrelief currently covers almost 12 % of the Zofin forest. Besides tree uprooting, the forest has high soil diversity that seems to be unique (Samonil et al., 2011). The soil heterogeneity can be found on a small scale that could not be explained by the soil properties and general soil evolution alone. Presumably, tree uprooting is a major influencing factor on the high soil variability. But a correlation between them could not be detected yet. More details about short- to long-term soil redistribution are required. To relate such values in a better context, surface age and, thus, the age of the soil should approximately be determined.

Figure 1: Tree uprooting in the Zofinsky forest. (M. Egli, 2017)

1.1.   Background

The microrelief of a tree uproot consists of a pit and mound. It has an important influence on infiltration efficiency, soil moisture, tree-water supply as well as seasonal microhabitat for specific soil fauna and forest stand resilience (Valtera and Schaetzl, 2017). It is known that TUR increases biological and ecological diversity in the forest (Samonil et al., 2008). Additionally, it has an essential impact on spatial variability and soil formation (Samonil et al., 2011, 2010a; Schaetzl, 1990). Tree uprooting can promote denudation in the short-term due to bioturbation and downslope transport. Its effects can stabilise slopes over longer timescales. The latter occurs because pits may serve as sediment traps, and mounds are often stabilised by vegetation. Despite this general knowledge many uncertainties and open questions remain. In particular, detailed knowledge about the effect of tree uprooting on soil development is limited due to little research on these dynamics. One reason for that is the small number of dated tree uprooting events even though tree uprooting and their morphological features are still visible in the landscape after

Introduction

several years. To understand the involving process, it is crucial to know the age of these events to be able to understand their effect on the landscape.

Different methods were used to date tree uprooting microrelief so fare. All of these methods include some unknown assumptions. Samonil et al. (2013) used dendrochronological dating. Tree census was used to date young uprooting (> 37 years), radiometric dating to date events younger than 200 years (especially ^{210}Pb) and for older morphological features radiocarbon dating (^{14}C) was applied. The cross-validation of the different methods give a maximum-overlap and therefore, a high probability of the dating and minimizing of the unknown assumption mistakes. Furthermore, tree uprooting has strong biomechanical effects on soils, and a substantial amount of soil material is moved downslope, sometimes even upslope or is simply ploughed. Samonil et al. (2017a) estimated several m³ (or Mg) ha^{-1} yr^{-1} that is affected by biomechanical processes. They proposed a humped conceptual model for biomechanical effects of trees in old-growth central European temperate forests with the highest activity at about 1000 m a.s.l. that decreases with higher and lower altitudes.

In this study nuclides such as ^{10}Be and fallout radionuclides are used to date morphological features without organic components and to derive erosion rates along slopes where tree uprooting has occurred. The nuclide ^{10}Be covers a long-time range from 10^3 to 10^6 years. With ^{10}Be, dating up to 1 Ma and the determination of long-term erosion rates is possible. Fallout radionuclides (FRN), however, indicate short-term processes, because their maximum emissions have occurred in the year 1964. FRN therefore are an effective approach to determine soil erosion rates for about the last 60 years (Lal, 2001).

The oldest so fare measured microrelief of a tree uproot exceeds 6000 years in Michigan. In this study six other microreliefs were measured that are over 4000 years old using radiocarbon dating. In Europe Samonil et al. (2013) could measure maximum ages of 1700 years. These ages show that the age of the microreliefs of a tree uproot are site specific and can differ widely.

In managed forests fewer tree uprooting events can be found. Due to the fact of timber production and costs they are not desired and prevented. When comparing the size of the tree uprooting events between managed and unmanaged forests not only the number but also the scale is different. The events in managed forests tend to be smaller since less large trees that are more prone to tree uprooting occur in managed forests (Valtera and Schaetzl, 2017). Further knowledge about the interactions between soil and trees for the soil development may change future forest management. Mainly due to the little knowledge about the interaction between soils and tree uprooting events, the long-term effects of these dynamics are uncertain. However, some

researches suggests possible positive feedback of tree uprooting on soil development (Samonil et al., 2010a; Valtera and Schaetzl, 2017). Therefore, tree uprooting should be considered in future forest management and furthermore in the evaluation of the naturalness of forest ecosystems.

In this thesis we focus on an unmanaged forest in the Czech Republic which has been the focus of major research projects. With the help of our results a broader and deeper understanding of the processes in our study area should be achieved.

1.2. Tree Uprooting

Tree uprooting (also called 'tree-throw') is a type of very intense bioturbation that has a significant influence on soil heterogeneity. Heavy wind or other physical stress is leading to root failure and uplifting. The tree is falling, and the root system is lifted up. The resulting morphological features are microreliefs defined as pit and mound (Figure 2).
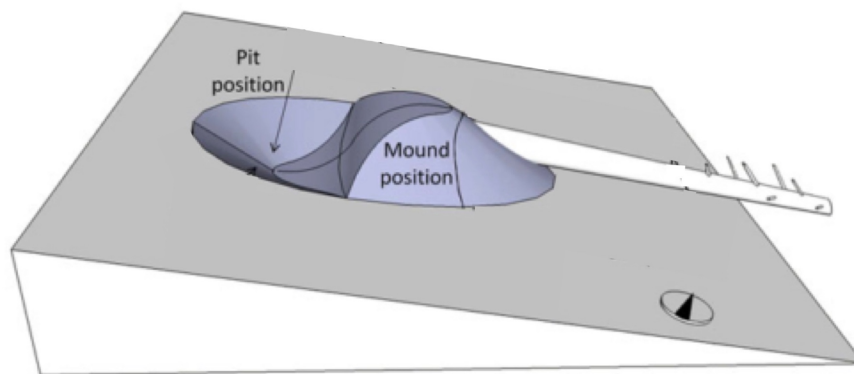
Figure 2: Schematic tree uprooting with pit mound microrelief and with the uprooted trunk. (Edited version from Samonil et al. 2015)

The size of the pit is irregular and depends on the size of the root system that is uplifted. Samonil et al. (2013) estimated an average size of fresh uprooting features of 5.9 m² including five different temperate forests. Besides the Zofin forest also the Razula reserve in the Czech Republic and three forest sites in Michigan were studied for this estimation. With the help of uprooted material, they could also calculate a rotation period of approximately 1380 years for these sites. After time pits often serve as sediment traps and collect water. For forest hydrology the pits are very important (Valtera and Schaetzl, 2017). Due to the filling of sediment the microrelief of typical pit-mound changes and the pit vanishes. The Mounds consists of new material that is exposed to the surface. Their shape is irregular. Some of the material from the mound falls down and is washed into the pit or down the slope. It is decreasing over time due to rooting of the root system, the loss of stability and the erosion of the soil. On the short-term the mound causes denudation. But on the long-term, it is proofed that slope stabilization develops and the mound is covered with

vegetation. Apart from that the long-term effect of the development of the microrelief is still unknown.

Depending on size and kind of tree, the time of total vanishing of the trunk due to rotting differs. After total rotting the pit-mound microrelief is the only visible sign indicating a past tree uprooting. With the help of dendrochronology, tree uprooting can be dated if the trunk is still existing. Afterwards, other methods like surface exposure dating or fallout radionuclides measurements must be used to date the older tree uprooting. For a better understanding, we will always talk about tree uprooting independent of the age and visible signs.

The age of so fare dated tree uprooting is varying between 200 to 2000 years in average. There were measured in different biomes worldwide except in tropical rainforests and deciduous forests in Africa and South America. The oldest tree uprooting is 6000 years and was measured in Michigan. A wide range between the longevity of tree uprooting microrelief exists based on site-specific conditions. Hence they need to take into account if tree uprooting wants to be examined. Besides the age of the tree uprooting also their rotation periods are measured in natural forests. Samonil et al. (2014) calculated a rotation period between 1250 to 1380 years with undisturbed conditions for Central Europe. Taking erosion and sedimentation into account, the rotation period reduces from 1380 to 870 years (Samonil et al., 2014, 2013). The rotation periods for Alaska are much smaller with 200 up to 400 years (Samonil et al., 2016). As well as the age of tree uprooting the rotation period varies based on site-specific conditions. Moreover, a comparison between different values must consider the different used dating techniques (Samonil et al., 2010a). Further data is needed.

The whole event of a tree uprooting interrupts the generally slow but progressive soil evolution. Tree uprooting mainly affects soil horizonation, as it mixes material that was originally systematically stratified (Samonil et al., 2015). Two types of effect on the soil can be distinguished. With a gentle or moderate slope mostly a mixed or contorted horizonation occur. The second type can be found on steep slopes where the horizons are inverted, and no or little mixing occurs (Schaetzl, 1986).

Although there are suggestions that tree uprooting rejuvenates the soil of the whole landscape (Kooch et al., 2015) the knowledge of the effect of the tree uprooting on the soil development is still insufficient. Quantitative values about soil erosion (or accumulation) induced by tree uprooting along hillslopes are almost inexistent.

1.4. Study Area

This study has been conducted in the Zofin forest, located in the south of the Czech Republic close to the border to Austria at a latitude of 48°39′58″ and longitude of 14°42′28″ (Figure 3). As the 4th oldest forest reserve in Europe, the studied core zone of Zofin has been under strict protection since 1838. It is part of the global network of forest research plots ForestGeo (http://www.forestgeo.si.edu/). Historical documents suggest that in this area lumbering has never occurred even before the protection (Samonil et al., 2015). The reserve contains 102 ha and is located at a mean altitude of 730 – 837 m a.s.l. The mean annual temperature is 4.3° C, mean annual precipitation of 900 mm and the mean slope is 8.6°. The parent material is granite, and the predominant soils are Cambisols, Podzols and Gleysols. The main tree species in the (spruce)-fir-beech forest are *Fagus sylvatica* L., *Picea abies* (L.) Karsten and *Abies alba* Mill. Tree census survey started in 1975 and was repeated almost every eight years with the last survey in 2008. The forest was strongly affected from the Kyrill hurricane on 18 January 2007 that caused many tree uprootings (Figure 4).

A very high soil variability on a small scale could be found in previous studies. With normal soil evolution, this high variability cannot be explained. The main important disturbance factor could be tree uprooting. Over 1000 tree uprooting microreliefs were analysed in this forest. 1289 pit-mounds were indirectly dated and 237 directly dated. Currently, 11.65 % of the forest of the research area is covered with tree uprooting pit-mounds, 7.7 % of them consisting of mound areas and 4.0 % of pit areas. Figure 5 shows the distribution of tree uprooting events over the whole forest reserve. The maximal observed pit-mound longevity found in this area is 1690 years (Samonil et al., 2017; Samonil et al., 2017; Samonil et al., 2014, 2011).

Figure 3: Map of the Czech Republic with study area Zofin. (Edited from OpenStreetMap)

Figure 4: Several tree uprooting caused by the Kyrill storm 2007. (T. Steinert, 2017)
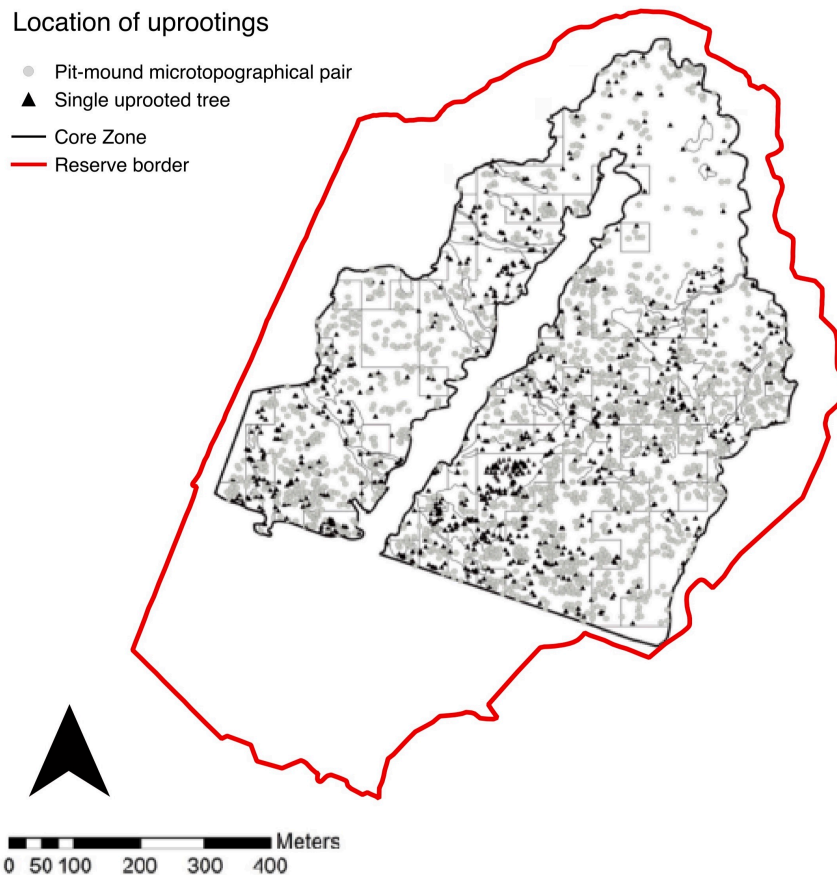
Figure 5: Location of tree uprooting microrelief (pit-mound) with and without the uprooted tree in the core zone of Zofinsky forest. (Edited version of P. Samonil)

1.5. Surface Exposure Dating and Determination of long-term Erosion

1.5.1. In Situ ¹⁰Be

Beryllium-10 (^{10}Be) is a radioactive cosmogenic isotope produced via interactions of high-energy cosmic radiation with target nuclei in the atmosphere ('meteoric') and the Earth's surface ('in situ'). As soon as the nucleus reaches the surface, a nuclear reaction is induced with an oxygen atom (O) (Schaetzl and Thompson, 2015). This reaction creates "cosmogenic isotopes", one of them being ^{10}Be. The surface exposure dating (rock surface dating) relies on terrestrially formed nuclides in solids. Therefore, the concentration of ^{10}Be can determine the time since when a rock is exposed to the surface. Boulders that are still connected to the bedrock are so-called "tor" landforms. The speed of the tor exhumation and therefore the different ^{10}Be concentration with depth can be used to derive surface lowering and, thus, soil erosion rates over a given time period (Raaba et al., 2018).

However, the so-called preexposure must be taken into account. The determined ¹⁰Be can be influenced by previous accumulation of ¹⁰Be through the uppermost soil layers. Therefore, the ¹⁰Be concentration can be slightly higher than the actual time of exposure. This pre-exposure needs to be considered during sampling and the analysis (McHargue and Damon, 1991).

1.5.2. Meteoric ¹⁰Be

Meteoric ¹⁰Be is produced similarly like in sit004e ¹⁰Be, but instead on the Earth's surface, the nucleus reacts already in the atmosphere ('meteoric') with an oxygen atom. With precipitation, meteoric ¹⁰Be is scavenged and deposited on top of Earth's surface where accumulates in the soils. Usually, highest concentration can be found in the upper soil layers from where it decreases with depth. ¹⁰Be may be transported downwards to the B and C horizon by infiltration and leaching following the weathering front (Figure 6) (Egli et al., 2010; Willenbring and von Blanckenburg, 2009). In this thesis, the non-steady-state approach is used for the estimation of soil erosion rates. With consideration of the estimated soil erosion rates and with the assumption of no erosion a possible age range of the soil can be calculated with help of a scenario calculation.

Figure 6: Schematic diagram of a soil profile and the different accumulation processes of ¹⁰Be into the soil. (Willenbring and von Blanckenburg, 2009)

1.7. Fallout Radionuclides

With help of fallout radionuclides (e.g. [137]C, ^{210}Pb, [239+240]Pu) soil redistribution can successfully be measured worldwide since the 1970s. Plutonium (Pu) is a fallout radionuclide that was globally distributed in the atmosphere during the thermonuclear weapon testing between 1953 and 1964. The half-life of [239]Pu is $t_{1/2}$=24'110 years and for [240]Pu $t_{1/2}$=6'563 years (Ketterer and Szechenyi, 2008). With precipitation and dry deposition, it accumulates in the soil. The timing of the main global fallout influences the time of Pu accumulation in the soil and therefore the potential time of soil redistribution. The Pu is strongly absorbed by clay particles in the soil (Hu et al., 2010; Zapata, 2002). The global fallout of Pu for the Southern Hemisphere is slightly smaller and less homogenous compared to the Northern Hemisphere with 0.185 ± 0.047 and 0.180 ± 0.014, respectively (Kelley et al., 1999). Based on the fallout, the amount of Pu and therefore short-term soil redistribution can be detected between 25 and 60 years.

1.8. Aggregate Stability

Aggregates are an assemblage of soil particles. Depending on the aggregate size they are more prone to erosion. Small aggregates are generally more stable than larger ones. Large aggregates can resist some erosion energy owing to their size and weight. In general soils with a high silt content have the highest potential for erodibility because the heavy sand particles and the binding clay particles are not dominant (Morgan, 1999). The clay particles have a high binding effect for elements in the soil. Therefore, they hold the aggregates together and protect them from erosion. Furthermore, organic matter is important for the degree of erodibility. Organic matter contributes to the stability of aggregates. A too high organic matter concentration (above about 15 – 20 %) however decreases the stability of aggregates. Additionally, a high amount of organic material on the forest floor is like a protecting layer for the aggregates and the soil below (Weil and Brady, 2017).

1.9. Research Questions and Hypotheses

The study site was and is part of previous and ongoing research activities about the influence of tree uprooting and tree – soil interaction from Prof. Pavel Samonil (Silva Tarouca Research Institute and Mendel University in Brno; Czech Republic). As a result, it is assumed that tree uprooting is a primary mechanism of downslope mass movement that influences soil variability in the Zofinsky forest. So far, quantitative values about soil erosion (or accumulation) induced by tree uprooting along hillslopes are almost inexistent. Even though it is known, that the exposure of bare soil promotes erosion as it happens after tree uprooting.

For a better process understanding of tree uprooting on soil evolution, this master thesis focuses on short- to long-term soil redistribution. To relate such values in a better context, surface age and, thus, the age of the soils will also be determined.

The long-term soil redistribution rates will be quantified using surface exposure dating of exhumating tors. We assume that the related surface lowering is predominantly corresponding to soil erosion. The short-term soil redistribution will be quantified by $^{239+240}$Pu, aggregate stability and the δ^{13}C approach. Soil ages will be estimated using meteoric ^{10}Be. Due to previous results, the soil profiles were predefined, described and chemical analyses already available. Supplementary we will measure the elemental contents with X-ray fluorescence (XRF).

Based on previous knowledge the main hypotheses are the following:

(1) The soils are very old and predominantly undisturbed, since the Zofin forest was not glaciated during the last glacier maximum.

(2) Erosion rates can even be detected in forested areas. The hypothesis that soil redistribution is close to zero in forested areas cannot be sustained.

(3) The present-day erosion (or soil redistribution) rates match long-term rates.

(4) The aggregate stability at a forest site is high.

Based on our goal the following research questions build the basis of this master thesis:

1) How old are the surfaces and consequently the soils in the Zofin forest? How precise is this determination?

2) Can we detect short-term erosion rates in the forest (due, among other things, by tree uprooting)?

3) How do these short-term soil redistribution rates relate to long-term rates?

4) Can we date some of the (visually examined) old tree-uprooting events?

2. Methods

2.1. Samples

This study was performed in the Zofinsky primeval forest. Three soil profiles were selected together with four tree-uprooting (TUR) sites for in situ ^{10}Be and one tor for the estimation of long-term erosion rates. Pu and aggregate stability samples were taken around the profiles.

2.1.1. Soil Profiles

Three different soil profiles (Figure 12) that were assumed to be undisturbed were sampled. These were used as reference sites for a comparison of sites affected by TUR.

In each soil profile, the main horizons were sampled for the determination of meteoric ^{10}Be, δ^{13}C and total elemental contents. Prof. Samonil sampled the soil profiles during previous projects. Basic analyses like pH, bulk density and the amorphous and crystalline element content were measured at the Laboratory of Morava in Studénka (the Czech Republic). The grain size distribution was measured at the Laboratory of K-Geo in Ostrava (the Czech Republic). The used methods are described in corresponding papers (Samonil et al., 2010b).

2.1.2. Soil Samples

For plutonium (Pu) measurement and the soil aggregate stability, additional soil samples needed to be sampled. The Pu samples were taken near each soil profile at a reference site and an erosion site (Figure 7 & 9). The reference sites were chosen at a flat undisturbed area where no erosion or deposition should have taken place (Figure 7). The erosion sites were located on a slope with indications for erosion (Arata et al., 2017). Additionally, one sample was taken at the mound of a TUR close to profile 61. At the TUR the tree trunk was already rotten, just the tree uprooting microrelief could be identified in the field. This sample should give us information about the soil redistribution of the mound. At each site four different depths, each having a 5 cm increment, were taken with the help of a soil core sampler of a volume of 100 cm^3. Each site consists of four sample replicates approximately 50 cm apart from each. In total 28 different site samples (including replicates) with four depths were sampled. The soil aggregate samples were taken around the soil profiles. At each profile, four replicates around 250 g of the upper 5 cm without the organic layer were taken.
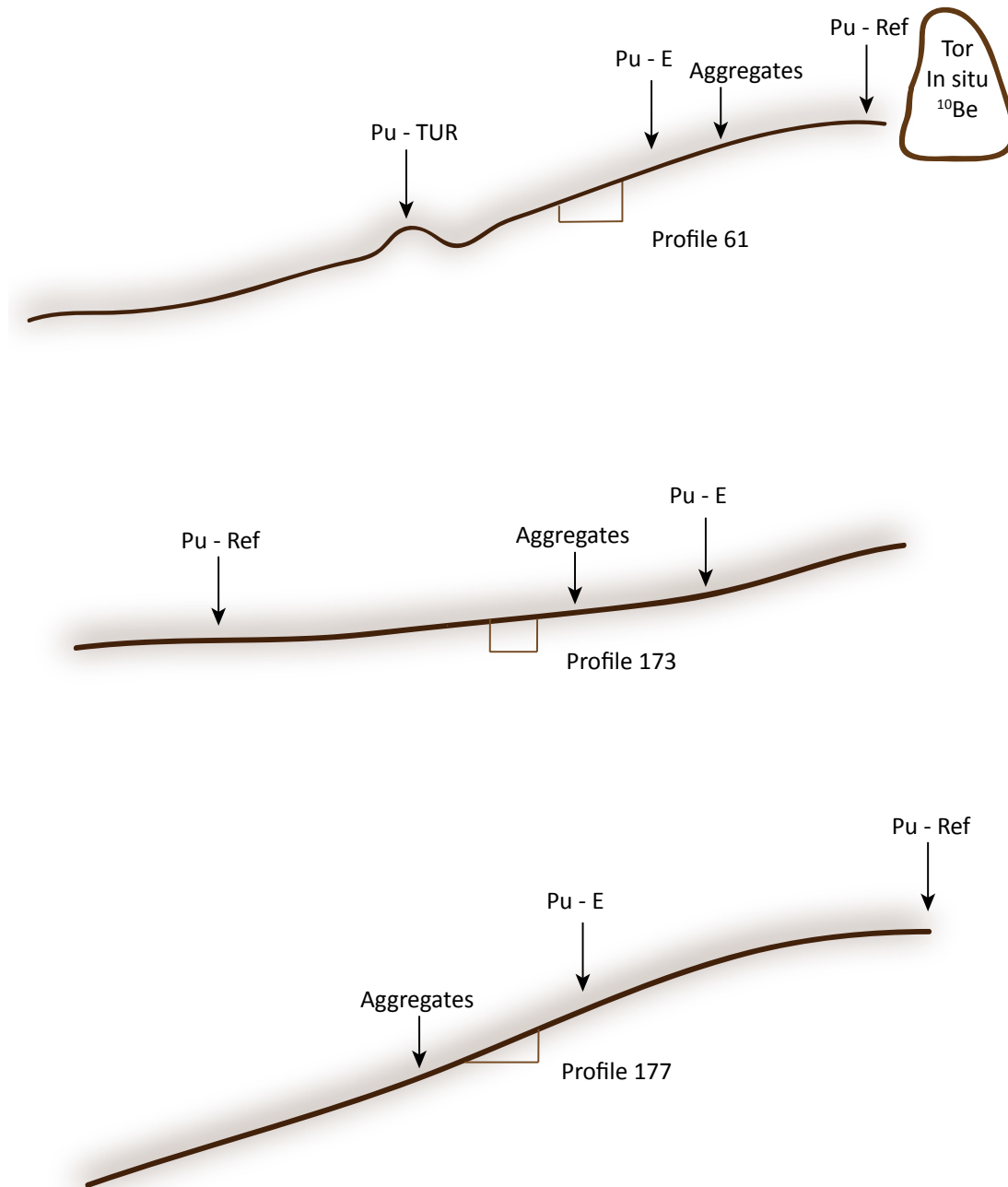
Figure 7: Schematic sampling site for all soil sample and the tor sampling. Pu – Ref = Plutonium reference site, Pu – E = Plutonium erosion site, Pu – TUR = Plutonium tree uprooting site, Aggregates = Soil samples for aggregate stability.

2.1.3. Rock Samples

Granite boulders need to be sampled to be able to detect cosmogenic [10]Be since this is produced in quartz. Every rock was cleaned from any moos before sampling. With a stone saw a chessboard pattern was sawed into the rock (Figure 8). With the help of a chisel and a hammer, the rock fragments were extracted. For each sample 1 – 2 kg of rock per sample were taken.

To determine the surface lowering as a result of long-term erosion a transect of one tor was sampled at three different heights at 10, 110 and 180 cm. Additionally, four 'boulders' (or rather

rocks) were sampled close to the profile 177 (Figure 9). They were located in old TUR where the tree was already rotten. These samples should give us an idea about possible ages of old TUR. Pre-exposure of the rocks might have occurred and disturbs the measured values. To have an indication of possible pre-exposure age of these stones, one sample was also taken below ground at a depth of 20 cm in the profile 177. At each sample following information were collected: latitude, longitude, elevation, dip angle, shielding, sample thickness and sample density. This information is needed to calculate the exposure age (see Chapter 2.2.2.1.).

Figure 8: Still visible chessboard pattern at the tor for in situ ^{10}Be after sampling. (T. Steinert, 2017)
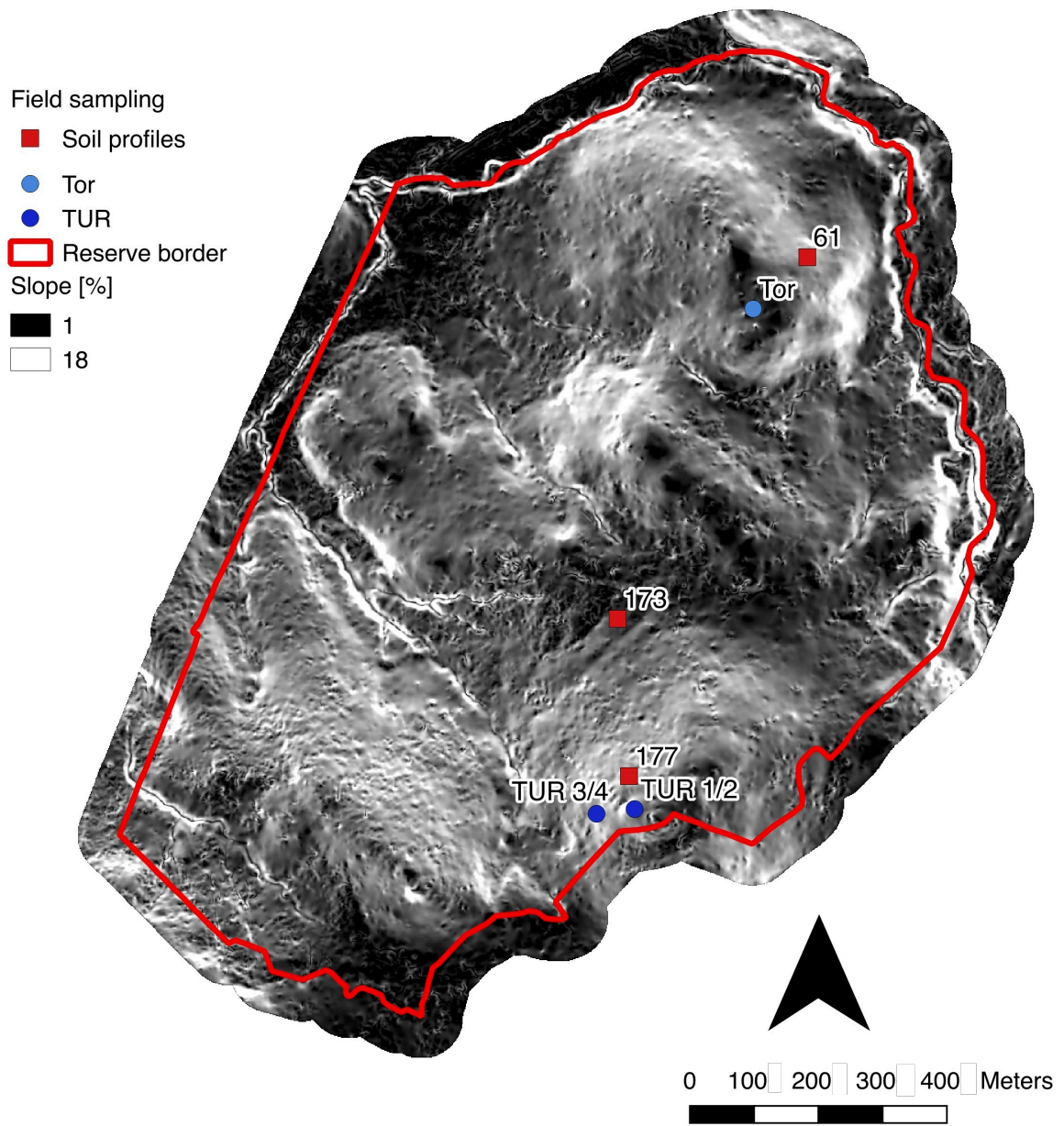
Figure 9: Zofinsky primeval forest reserve with soil profiles and rock samples (Tor and TUR).

2.2. Sample Preparation and Measurements

The sample preparation in the laboratory was conducted according to the lab procedure of Egli et al. (2015).

2.2.1. Preliminary Preparation Before Measurements

All the soil and rock samples were dried for 48h at 70° C. For further analysis the soil samples were sieved to 2 mm to separate the fine earth fraction and the skeleton. Additionally, some subsamples were milled in a tungsten carbide vessel.

2.2.2. Surface Exposure Dating Using ^{10}Be

2.2.2.1. In Situ 10Be

The rock samples were crushed with the rock crusher and sieved to the fraction 0.5 – 1 mm. About 2 x 200 g of the fraction were covered with Aqua Regia, washed and dried in the oven. Thereafter, the Feldspar was removed by froth flotation. In a next step, the samples were leached for one week with hydrofluoric acid (HF) in a shaker to obtain pure quartz. Afterwards, the sample was dried in the oven. ^{9}Be$(NO_3)_2$ was added to the sample and dried again. 10 ml Millipore water was then added the sample was heated for 1h at 80° C to dissolve the BeF$_2$. The liquid was collected in centrifuge tubes, and 13.2 ml of HCl (32 % v/v) were added. Afterwards, the Fe was removed with an anion exchange column and heated until the sample was completely dry. To dissolve the sample, oxalic acid (0.4 M) was added to the sample and beryllium was separated from Al using cation exchange columns, where Al formed complexes with the oxalic acid that absorbed in the column. The sample was heated at 80° C to reduce the volume to about 10 ml and Be(OH)$_2$ was precipitated using NH$_4$OH. The gel was then dried in the oven at 70° C overnight and heated at 200° C on a heating plate. In the end, the gel was calcinated for 2 hours at 850° C in the oven to obtain BeO. Finally, the BeO was mixed with Nb powder and pressed into a sample holder for accelerator mass spectrometry (AMS).

The ^{10}Be/^{9}Be ratios were measured at the ETH Zurich AMS system Tandy (Christl et al., 2013) and normalized to the ETH Zurich in house AMS standard S2007N (^{10}Be/Be = 28.1 x 10^{-12} nominal) which has been calibrated relative to ICN 01-5-1 (^{10}Be/^{9}Be = 2.709 x 10^{-11} nominal) (Nishiizumi et al., 2007) both associated with a ^{10}Be half-life of 1.387 ± 0.012 My (Chmeleff et al., 2010; Korschinek et al., 2010).

With help of the information listed in Table 1, the surface age of each rock was calculated. The calculation was done using the CRONUS 2 online calculator provided by the Cosmogenic Nuclide Lab (2016).

Table 1: All values observed from the field or in lab work that are needed to calculate the exposure age according to CRONUS 2.

Field	Units	
Sample name	Text/ Code	Additional notes
Latitude	Decimal degrees	
Longitude	Decimal degrees	
Elevation	m a.s.l.	
Shielding		Angle of azimuth
Sample thickness	cm	
Laboratory	**Units**	
Shielding correction factor		Calculated out of azimuth and exposition of the sample
Carrier	g	Amount of carrier that was added to each sample
Rock erosion rate	cm/year	
^{10}Be concentration	Atoms/g	
Uncertainties in nuclide concentrations	Atoms/g	

The erosion rate on long-term was calculated with help of the height and the measured ages of the tor (Figure 10). The tor was once covered with soil. With soil erosion, the surface lowered and exposed the tor. This erosion rate is used for scenario calculations with the meteoric ^{10}Be ages.

$$Erosion\ rate = \frac{\Delta t}{\Delta h} * \rho$$
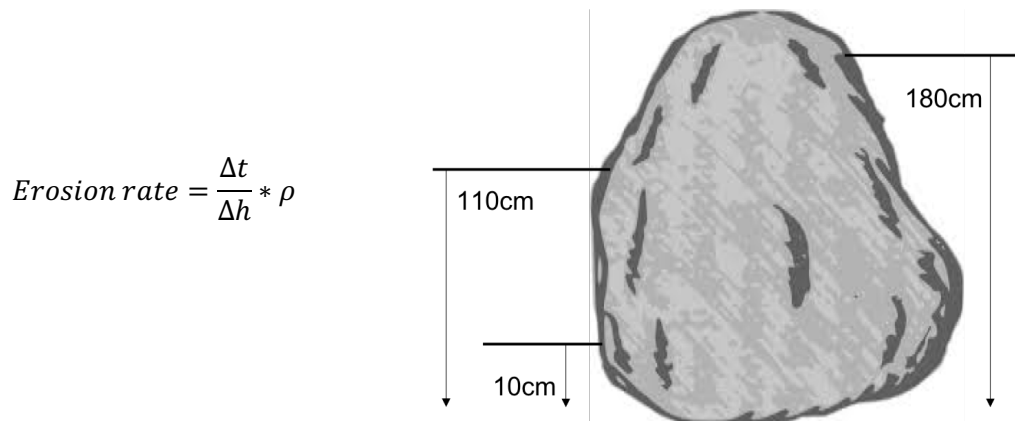
Figure 10: A schematic graph with sampling heights at the tor.

2.2.2.2. Meteoric ^{10}Be

Meteoric ^{10}Be was extracted from the soil samples using a modified method from Horiuchi et al. (1999) and Egli et al. (2010). About 2 g soil sample (< 2 mm fraction) were needed for meteoric ^{10}Be. The sample was heated at 550° C for 3 h to remove organic matter. 1 mg of ^{9}Be(NO$_3$)$_2$ (carrier) and 8 ml of HCl (16 % v/v) were added to the sample, and leached overnight in a shaker.

Methods

The sample was subsequently centrifuged and the liquid was collected. 5 ml of HCl were added to the solid part and leached overnight a second time. Thereafter, the liquid was collected together with the first leachate and heated at 80° C to reduce the volume to ca. 10 ml. In a next step, NaOH (16 % v/v) was added until the pH reached the value of 2. To complex metals such as Fe and Mn, 1 ml of an aqueous solution containing 10% EDTA was added. The pH value was then increased to 8 by adding NaOH to precipitate the gel containing $Be(OH)_2$ and $Al(OH)_3$. NaOH was added to the gel to reach a pH value of 14. $Be(OH)_2$ and $Al(OH)_3$ re-dissolved in the solution that was separated from the gel by centrifugation. HCl was added again to the solution to reduce the pH value to 2 and thereafter 1 ml of EDTA. The gel containing $Be(OH)_2$ and $Al(OH)_3$ was precipitated with NH_4OH and centrifuged. To dissolve the sample, oxalic acid (0.4 M) was added to the gel and beryllium was separated from Al using cation exchange columns, where Al formed complexes with the oxalic acid that absorbed in the column. The sample was heated at 80° C to reduce the volume to about 10 ml and $Be(OH)_2$ was precipitated using NH_4OH. The gel was then dried in the oven at 70° C overnight and heated at 200° C on a heating plate. In the end, the gel was calcinated for 2 hours at 850° C in the oven to obtain BeO. Finally, the BeO was mixed with Nb powder and pressed into a sample holder for accelerator mass spectrometry (AMS).

The [10]Be/[9]Be ratios were measured at the ETH Zurich AMS system Tandy (Christl et al., 2013) and normalized to the ETH Zurich in house AMS standard S2007N ([10]Be/Be = 28.1 x 10^{-12} nominal) which has been calibrated relative to ICN 01-5-1 ([10]Be/[9]Be = 2.709 x 10^{-11} nominal) (Nishiizumi et al., 2007) both associated with a [10]Be half-life of 1.387 ± 0.012 My (Chmeleff et al., 2010; Korschinek et al., 2010).

The resulting [10]Be concentrations and their depth for each profile indicate the deposit distribution by depth. With help of the scenario, we are able to get a possible age range for our soils. In the scenario, the precipitation needs to be adjusted depending on the precipitation rate during the soil development (Egli et al., 2010; Lal, 2001; Maejima et al., 2004; Zollinger et al., 2017, 2015).

Scenario calculation

The equation for determining the exposure age of a soil was used from Maejima et al. (2004):

$$t = -\frac{1}{\lambda}\ln\left(1 - \lambda\frac{N}{q}\right),$$

where t is the age of soil, λ is the decay constant of [10]Be (4.997 x 10^{-7} year^{-1}), N is the inventory of [10]Be in time t (cm^{-2}) and q is the annual deposition rate of [10]Be (cm^{-2} year^{-1}) (Maejima et al., 2004). The deposition rate of [10]Be is so fare unknown. Up to now, it is estimated that the deposition rate of [10]Be for the past is proportional to the rainfall (Monaghan et al., 1985/1986). The present-day

precipitation rates in Zofin are assumed to represent the rates during more or less the whole Holocene. During the last ice age (Pleistocene) these rates are unknown. It is however known, that the climate was in general much colder and drier. Modeled precipitation rates during the last glacial maximum for the south of Czech Republic are assumed to be 25 – 75 % of the present-day precipitation (Heyman et al., 2013). To determine the exposure age of our soils we used a scenario calculation. The scenario was done with different assumptions. The precipitation rate is one assumption and range between the present-day precipitation rate and the assumed precipitation during the soil development. For this assumption, we used the equation:

$$P = P_{today} * F + P_{IA} * (1 - F); \ P_{IA} = \begin{Bmatrix} P_{today} * 0.25i \\ P_{today} * 0.75i \end{Bmatrix},$$

where P = precipitation rate (mm/year), F = precipitation proportionality factor and P_{IA} = precipitation rate during ice age/ soil development defined by the soil age with the assumption of no erosion. Besides the precipitation, the erosion rate also influences the soil age. Therefore, we calculated for each profile the soil age with and without erosion. The erosion rate is based on the calculation from the in situ ^{10}Be erosion rate (that equaled to 0.3 t/ha/year). For profile 173 we added a second calculation with 1 t/ha/year erosion rate. The different scenarios give us a possible age ranges of the investigated soils.

2.2.3. Fallout Radionuclides

The measurement of Pu followed the procedure of Ketterer et al. (2015). Four batches were prepared, including three blanks, two standards and five replicates as cross-validation. The milled samples are weighted into vials and dry-ashed in a muffle oven to remove all organic matter. Afterwards, a NIST 4334 g ^{242}Pu spike solution is added. By treating the samples with HNO_3 and then placing them into the oven, carbonate is dissolved and leached from the samples. After HNO_3 leaching, Pu is in the solution and needs to be separated from the solid soil particles by filtration through columns. To convert Pu into Pu($_{IV}$) oxidation state, $NaNO_2$ is added and heated to expel NO_2. Afterwards, the samples are preconcentrated by adding TEVA and rinsed through microcentrifuge tubes with a glass wool plug. In the end, Pu is eluted and the final solution collected. The Pu measurements were done using a QQQ-ICP-MS at the Chemistry Department of the University of Zurich.

Methods

With the Pu activity (Bq/kg) the erosion rate was calculated by several approaches. Among them is the profile distribution model (PDM) from Walling and He (1999):

$$"A'(x) = A_{ref}(1 - e^{x/h_0}),$$

where $A'(x)$ = the amount of isotope inventory above depth x (Bq/m²), x = depth from soil surface expressed as mass between top and actual depth (kg/m²), A_{ref} = reference inventory as mean of all reference sites (Bq/m²) and h_0 = profile shape factor that is a coefficient describing the rate of exponential decrease in inventory with depth, for soil profiles in uncultivated sites" (Zollinger et al., 2015). The difference to other equations is the inclusion of a coefficient describing the Pu value for the soil depth.

Additionally, the inventory method (IM) according to Lal et al. (2013) was used:

$$L = -\frac{1}{\alpha P}\ln\left(1 - \frac{I_{loss}}{I_{Ref}}\right),$$

with L = loss of soil (cm), $I_{loss} = I_{Ref} - I$, I_{Ref} = the local reference inventory as mean of all reference sites (Bq/m²), I = measured total inventory at the sampling point (Bq/m²) and P = particle size. Following the approach of Alewell et al. (2014), the coefficient α was obtained from a least squared exponential fit of the isotopes ([239+240]Pu) depth profile. The loss of soil can then be calculated to the erosion rate (t/ha/year). The equation models the exponential decrease of the Pu concentration with depth. Besides that, the equation takes into account that erosion tends to remove smaller particle size more easily and that this fine-grained material tends to have a higher [239+240]Pu activity due to the larger surface to volume ratio (Lal et al., 2013).

As a third method, the code 'Modelling Deposition and Erosion rates with RadioNuclides' (MODERN) of Arata et al. (2016) was applied. This is a new method to calculate the erosion or deposition rate using Pu values. MODERN is available as a package in R Studio. It is based on the assumption that the original soil layer changes in thickness over time.
The model allows adjusting multiple adaptions simultaneously for the reference depth profile to the site-specific conditions. First assumptions of past processes are necessary and need to be included in the simulation. As input values, the Pu concentration for each sampling layer of the reference site and the total inventory of the erosion or deposition site is needed. The output of the simulation is in cm/year and need to be transformed to t/ha/year for comparison with the PDM and the IM model. For this transformation, the mean bulk densities of the first two sampling layers (0 - 10 cm) are taken for the erosion or deposition site (Arata et al., 2016).

18

2.2.4. Elemental Composition

The available data from the laboratory at the Mendel University of Brno included the total C and N content along the soil profiles. The resulting data distribution was rather surprising. Therefore, we decided to redo these measurements using an elemental analyzer. Around 5 to 10 mg soil for each soil horizon were weighted into tin capsules to be measured in a combustion analyzer.

The samples were analysed by two different methods both based on the combustion method. One run was done using the Piccaro combustion module. Depending on the carbon content the OAS or the Chernozem standard was used for calibration and the calculation. For OAS ≈ 5 mg, for Chernozem ≈ 15 - 20 mg was weighted into aluminium capsules and burned. The used standard $\delta^{13}C$ concentration of the Chernozem is -25.978 ± 0.023 % and for total C 1.914 ± 0.005 %. The Piccaro combustion module measures the total C content and the $\delta^{13}C$ concentration.

The second run was measured using the elemental analyzer isotope ratio mass spectrometric (IRMS). For this method, only the Chernozem standard was used, which is suitable for carbon content less than 10 %. The IRMS detects the concentration of total C and N in percent, and the ratio of $^{13}C/^{12}C$ and $^{15}N/^{14}N$ ‰ (also called delta (δ) ^{13}C and ^{15}N). Compared to the Piccaro combustion module it gives us additional information about the N content and the isotopes.

2.2.5. Geochemistry (XRF)

The XRF measurements determined the total element concentrations in the soil samples. Approximately 5 g of the milled sample from each soil horizon was weighted in into capsules. The samples are irradiated with energy-dispersive X-ray energy. As a result, atom instability was forcing the electrons to reallocate themselves. During this reallocation, the atoms produce electro specific energy that is measured by detectors (Fitton, 1997).

2.2.6. Aggregate Stability

Approximately 20 mg of the sieved samples were in a first step put into deionized water for 10 minutes. All floating organic material was poured off and dried in the oven with the other samples. Afterwards, the liquid was gently decanted, the remaining soil material was sieved gently by hand on a column of four sieves: 1, 0.5, 0.25, 0.125 mm. They were treated with ethanol to decrease the additional aggregate breakdown during treatment (Le Bissonnais, 1996). After the wet sieving, each aggregate size was dried in the oven for 24 hours at 70° C and weighted after.

Methods

Figure 11: Aggregates in each size after the wet sieving and drying in the oven. (T. Steinert, 2017)

During storage the aggregates could have further broken down and change particle size. Because of same storage (in plastic bags, Figure 11) this mistake can be neglected in the analysis.

For the analysis the mean weight diameter (MWD) of all size classes from dry and wet sieving (> 5 mm until < 125 μm) was used. It is defined as:

$$MWD_i = \frac{\sum m_{wi} \times \bar{d_i}}{\sum m_i}; \qquad MWD = \sum MWD_i$$

with MWD_i = mean weight diameter of the "ith" sieve class, m_{wi} = sum of the mass fraction of soil remaining on each sieve after sieving (g), d_i = the mean mesh size of the "ith" sieve (mm) and m_i = the total amount of used sample weight (Nimmo and Perkiins, 2002).

Additionally, we tried to predict the MWD using the equation of Chenu et al. (2011). Out of 380 samples, they calculated a best fitting equation predicting the MWD. The main influencing factors that they include in the equation are organic carbon, clay content and a factor of the environment where the samples were taken. The environment is divided into cultivated and natural undisturbed soils (grassland and forest) with an environmental factor of -0.17 and 0.34, respectively (Chenu et al., 2011).

$$MWD = 0.34\,C + 0.008\,clay + environment$$

2.2.7. Grain Size

The grain size distribution was conducted at the external Laboratory of K-GEO in Ostrava, the Czech Republic. Due to results that did not appear meaningful, we decided during analysis to remeasure three horizons of the profiles in Zurich. Originally this measurement was not planned. Consequently, sample size and time was limited. The samples were measured at the Laboratory of K-GEO with the Casagrande method. We have to assume that organic matter was not destroyed prior to the analyses in the Laboratory of K-GEO and therefore is remeasured together with the clay content. To get a good cross-check despite the limitations, we decided to measure three different horizons, one in each profile. The horizons were selected at different depths and with a different organic matter in the original measured data.

Around 50 – 70 g of the fine earth fraction (< 2 mm) was heated with 3 % H_2O_2. The material was wet sieved to 32 µm through 8 different mesh sieve size. The < 32 µm fraction was further measured with X-rays by the Sedigraph 5100 to obtain the fraction distribution until 1 µm. For the whole grain size distribution, both results from the wet sieving and the measured X-ray data were merged.

3. Results

3.1. Soil Profiles

3.1.1. Profile 61

Profile 61 is located at a midslope position having a dip of 18°. It is located at 719 m a.s.l. with the coordinates 48.669° N/ 14.708° E. The soil type is classified as a Haplic Cambisol which is a 'young' developed soil with clearly visible but not fare developed subsoil. The sampled horizons in the field were Ah (0 – 15 cm), Bv (15 – 30 cm), Bv2 (30 – 50 cm), BvC1 (50 – 80 cm), C1 (80 – 100 cm) and C2 (100 – 140 cm). The diagnostic horizons are based on the KA5. The predefined horizons for all three profiles are visualized in Figure 12.
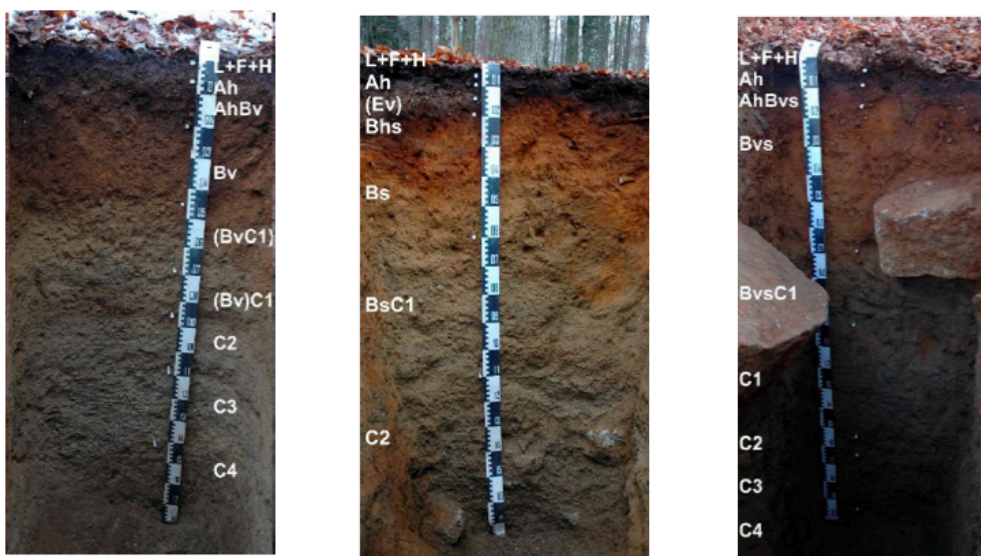
Figure 12: Soil profiles at the first excavation. From right to left: profile 61 (Haplic Cambisol), profile 173 (Albic Podzol), profile 177 (Entic Podzol) based on KA5. (P. Samonil, 2013)

3.1.2. Profile 173

The profile 173 is located at the bottom of a slope. The slope angle is 5.5° and the profile is located at 722 m a.s.l. with the coordinates 48.664° N/ 14.706° E. It is classified as an Albic Podzol which is an acid soil with eluvial, leached E-horizon. In the subsoil Fe-Al-humus-connections are accumulated (washed in). The sampled horizons in the field were Ah/E (0 – 10 cm), Bhs (10 – 14 cm), Bs (14 – 30 cm), Bs2 (30 – 50 cm), BcC1 (50 – 100 cm) and C2 (100 – 150 cm).

3.1.3. Profile 177

The profile 177 is located at the same slope as the profile 173 but further up at the beginning of the slope. The profile has a dip of 20°, and is located at 751 m a.s.l. with the coordinates 48.663° N/ 14.707° E. It is classified as an Entic Podzol. An Entic occurs typically on a steep slope compared to an Albic Podzol that occurs on flatter parts of the ground. The sampled horizons in the field

were AhBvs (0 – 15 cm), Bvs (15 – 30 cm), Bvs2 (30 – 50 cm), BvsC1 (50 – 100 cm) and C2 (150 – 160 cm).

3.2.   Surface Exposure Dating Using ^{10}Be

3.2.1. In Situ ^{10}Be

Close to profile 61, one tor at three different heights was measured. The sample at the height of 180 cm has an age of 66.7 ka, the sample at 110 cm 50.3 ka and the sample at 10 cm 15.9 ka. The erosion rate calculated by the measured ages is 0.3 t/ha/a.

To be able to date the possible pre-exposure of our rock samples located in old TUR, one rock in profile 177 was sampled at a depth of 35 cm below ground. The calculated age of this rock is 21.3 ka and was subtracted from the other rocks (corrected age, Table 2).

Table 2: Measured rock influenced by tree uprooting for in situ ^{10}Be measurement.

Sample	Age (ka)	Corrected Age (ka)
Rock at a depth of 35 cm (in profile 177)	21.3	0
TUR 1	42.1	20.8
TUR 2	30.1	8.8
TUR 3	32	9.7
TUR 4	34.5	13.2

Results

3.2.3. Meteoric ^{10}Be

The ^{10}Be concentration measured in the profile 61 shows a "zigzagging" curve (Figure 13). It increases from the top of the soil and has a maximum of 5.8 – 6.2 ^{10}Be atoms/g x 10^8 in the horizons Bv2 and C1. In between at BvC1 and C2, the concentration decreases to 4 ^{10}Be atoms/g x 10^8.
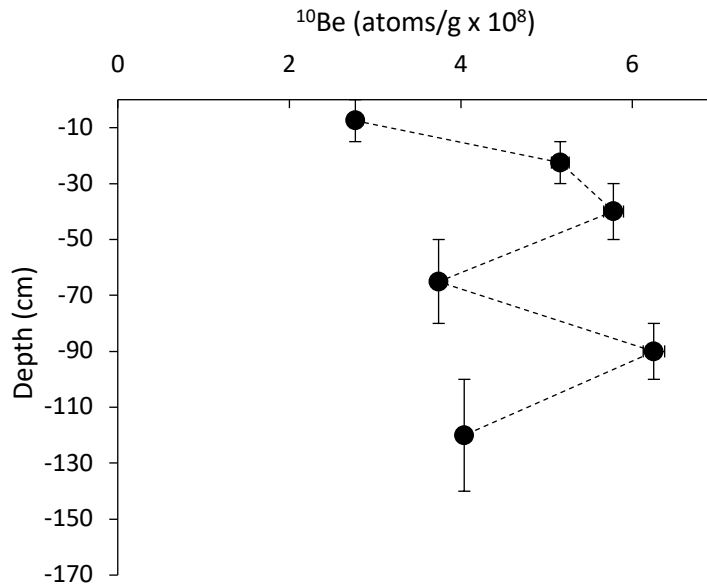
Figure 13: ^{10}Be concentration with depth in profile 61.

For the profile 61, the soil age with the highest likelihood is 44 – 90 ka assuming no erosion and an average precipitation rate of 810 mm/year. With an erosion rate of 0.3 t/ha/year the soil age ranges most likely between 74 to 210 ka (Figure 14).
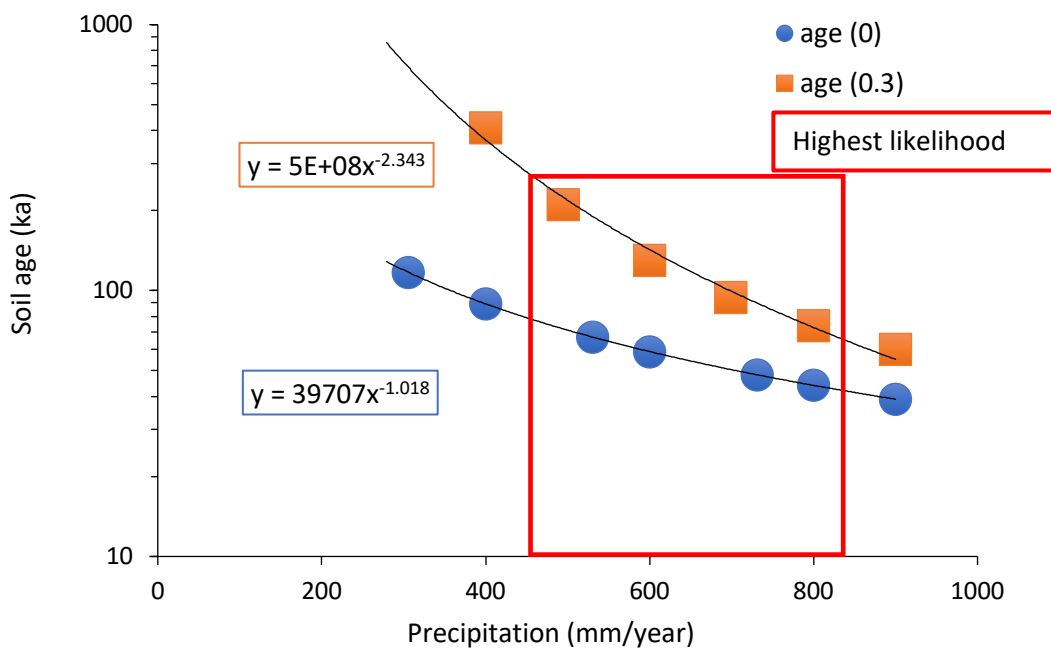
Figure 14: Scenario calculation for profile 61 with 0 and 0.3 t/ha/year erosion.

The meteoric [10]Be concentration in profile 173 starts low and increases to its maxima of 3.9 [10]Be atoms/g x 10[8] at Bs2. Afterwards, it decreases constantly (Figure 15).
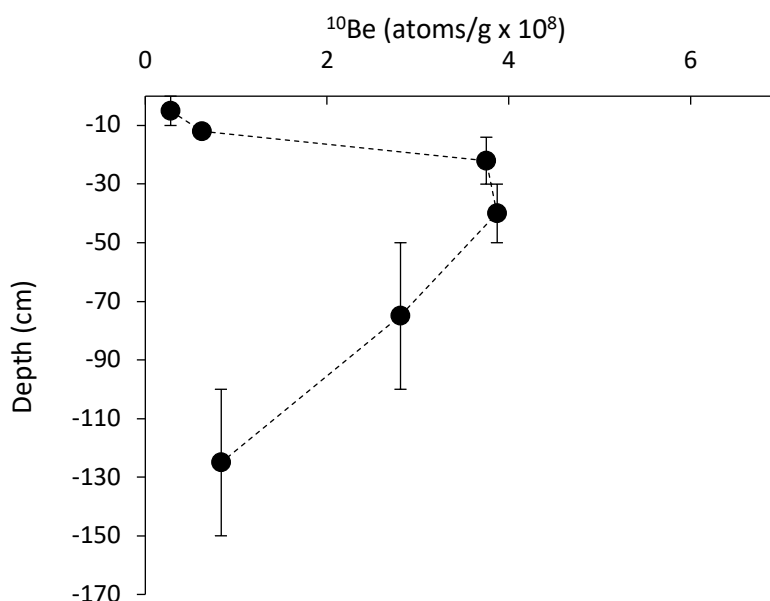
Figure 15: [10]Be concentration with depth in profile 173.

Using a scenario calculation, a soil age between 23 to 46 ka can be estimated with the assumptions no erosion and an average precipitation of 810 mm/year. With the assumption of an erosion rate of 0.3 t/ha/year, the age increases slightly to 23 – 55 ka. Due to the small difference we calculated an additional scenario with an erosion rate of 1 t/ha/year. The resulting age ranges between 29 to 71 ka (Figure 16).
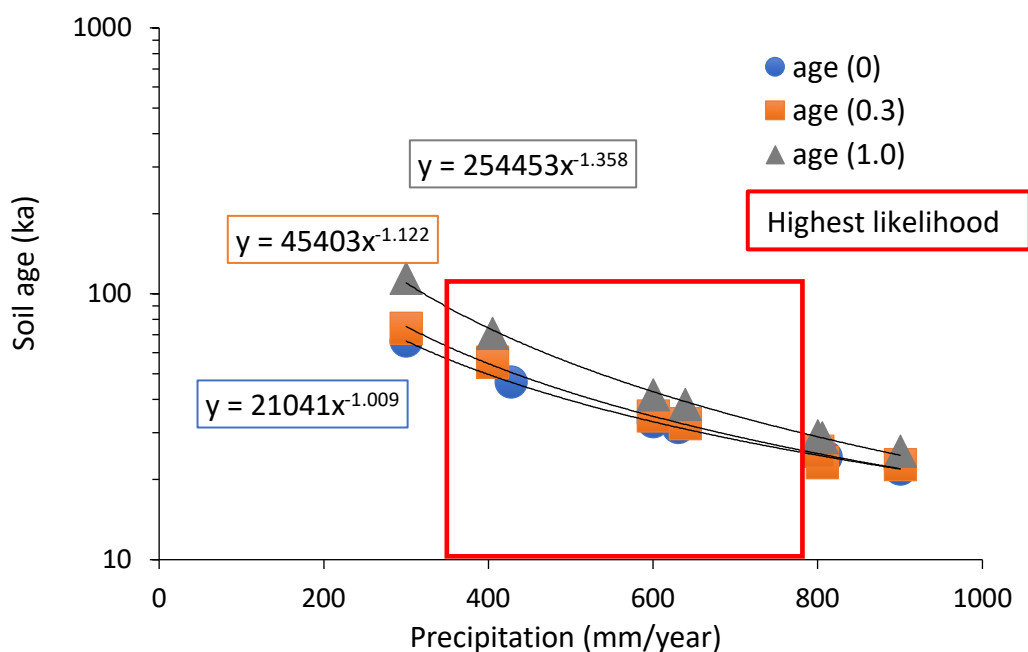
Figure 16: Scenario calculation for profile 173 with 0, 0.3 and 1 t/ha/year erosion.

Results

The meteoric [10]Be concentration in profile 177 starts low and increases in the horizon Bvs1. Afterwards, it decreases again constantly (Figure 17).
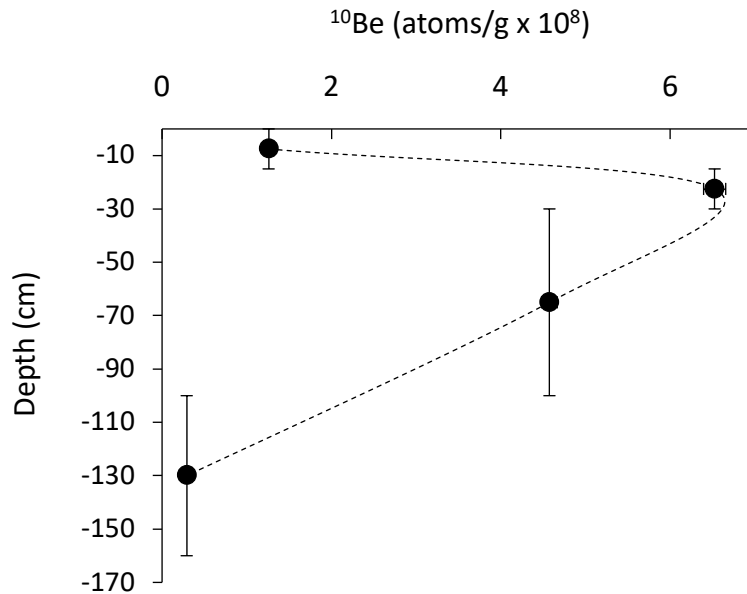
Figure 17: [10]Be concentration with depth in profile 177.

For this profile, the measurement of the sample for horizon BvsC1 did not work (although we tried to measure it three times). Therefore, the values between horizon Bvs2 and C2 had to be interpolated.

With the scenario calculation, a soil age between 34 – 50 ka with no erosion can be estimated. With the erosion rate of 0.3 t/ha/year, the soil age increases to 40 – 85 ka (Figure 18).
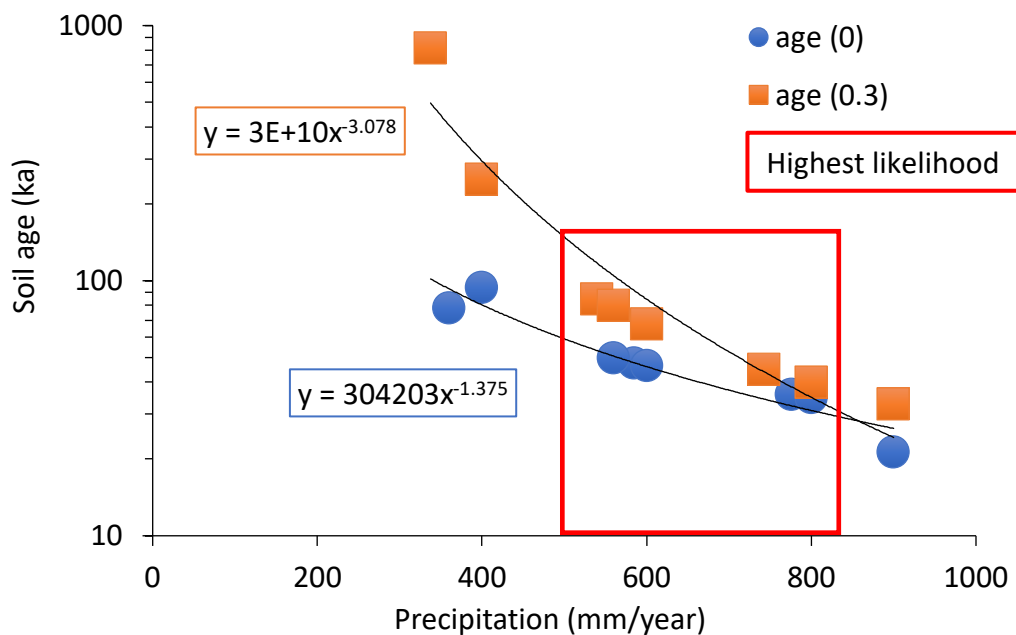
Figure 18: Scenario calculation for profile 177 with 0 and 0.3 t/ha/year erosion.

3.3.   Fallout Radionuclides

In all samples, a $^{239+240}$Pu activity could be measured. The results for the Pu inventories and the erosion rates calculated by the three different methods are presented in

Table 3 for all profiles. The results of the Pu inventory for each site are shown in Table 4 – 6.

Table 3: Results of Pu inventories and the erosion rates calculated with three different models. SM = section mass, PDM = profile distribution model, IM = inventory method and MODERN = modelling deposition and erosion rates with radionuclides, Ref = reference, E = erosion and TUR = tree uprooting.

Profile	Site	Inventory (based on SM) (Bq/m²)	Model PDM[a] (t/ha/year)	Model IM[b] P=1 (t/ha/year)	Model IM[b] P=1.2 (t/ha/year)	Model IM[b] P=1.5 (t/ha/year)	Model MODERN[c] (t/ha/year)
61	Ref	77.83 ± 15.33					
	E	60.86 ± 14.43	-1.11	-1.11	-1.02	-0.81	-1.49
	TUR	58.90 ± 13.25	-1.36	-1.66	-1.47	-1.18	-1.96
173	Ref	47.71 ± 11.67					
	E	39.02 ± 15.75	-0.83	-0.64	-0.59	-0.47	-0.68
177	Ref	36.45 ± 8.45					
	E	56.55 ± 13.08	1.09	1.25	0.98	0.79	1.05

Negative values = Erosion, Positive values = Deposition

[a] Walling & He (1999)

[b] Lal et al. (2013)

[c] Arata et al. (2016)

Results

The total inventory of the reference site of profile 61 is slightly higher with 77.83 ± 15.33 Bq/m^2 compared to the erosion and TUR site with 60.86 ± 14.43 Bq/m^2 and 58.90 ± 13.25 Bq/m^2, respectively. These inventories were calculated based on the section mass used in the PDM and IM model. The calculated erosion rates range between -0.81 t/ha/year to -1.49 t/ha/year in profile 61. The $^{239+240}$Pu activity in profile 61 constantly decreases with depth at each site (Figure 19).

Table 4: $^{239+240}$Pu activities (Bq/m^2) at profile 61 for each sample. Ref = reference, E = erosion and TUR = tree uprooting.

Sample site Profile 61	0 – 5 cm	5 – 10 cm	10 – 15 cm	15 – 20 cm	Inventory (Bq/m^2)
Ref 1	112.30	9.17	1.66	2.92	126.06
Ref 2	51.24	10.03	6.29	0.61	68.17
Ref 3	51.04	3.71	8.06	0.35	63.16
Ref 4	47.07	3.75	2.91	0.20	53.93
E 1	55.41	24.38	5.16	3.97	88.92
E 2	21.35	9.31	2.08	1.60	34.35
E 3	43.42	2.49	0.52	0.35	46.78
E 4	52.01	14.56	5.04	1.78	73.39
TUR 1	64.75	0.84	0.86	0.23	66.68
TUR 2	61.52	17.94	1.61	0.63	81.70
TUR 3	20.81	0.77	0.17	0.40	22.15
TUR 4	61.66	1.48	0.76	1.16	65.06
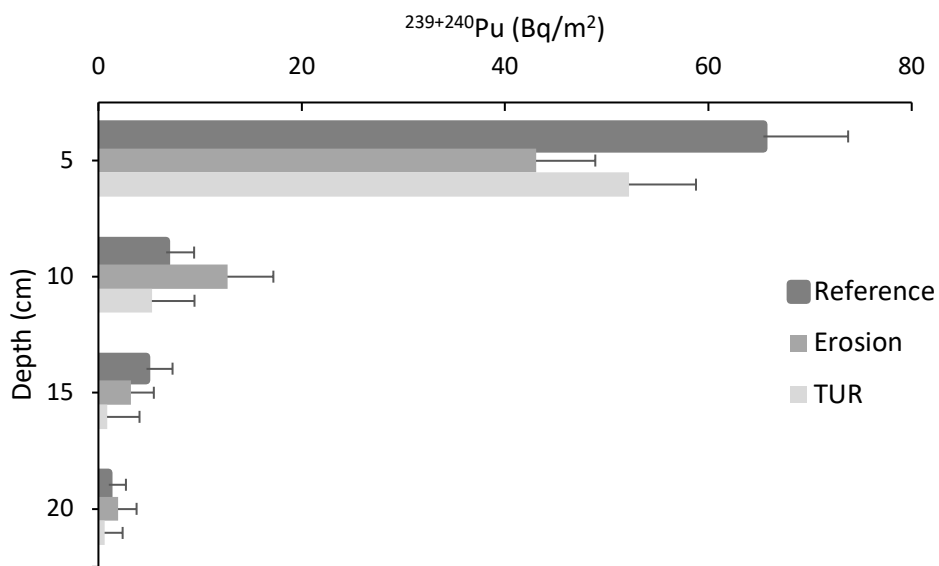
Figure 19: $^{239+240}$Pu activity with depth for samples of profile 61.

 At the reference and the erosion site of profile 173, the $^{239+240}$Pu activity decreases with depth, whereby the $^{239+240}$Pu activity is higher at the erosion site except for the first 5 cm (Figure 20). Nevertheless, the total inventory of the reference site is with 47.71 ± 11.67 Bq/m^2 higher than the erosion site with 39.02 ± 15.75 Bq/m^2. The calculated erosion rates range between 0.79 t/ha/year to 1.25 t/ha/year.

Table 5: $^{239+240}$Pu activities (Bq/m^2) at profile 173 for each sample. Ref = reference, E = erosion and TUR = tree uprooting.

Sample site Profile 173	0 – 5 cm	5 – 10 cm	10 – 15 cm	15 – 20 cm	Inventory (Bq/m^2)
Ref 1	10.28	3.20	1.16	0.44	15.08
Ref 2	54.37	10.99	3.99	1.06	70.42
Ref 3	45.51	7.70	1.61	0.74	55.55
Ref 4	38.43	8.81	1.60	0.94	49.78
E 1	21.00	4.08	2.73	4.31	32.13
E 2	46.78	7.98	5.11	0.87	60.76
E 3	5.50	4.94	8.05	2.84	21.34
E 4	5.00	21.17	13.39	2.29	41.84
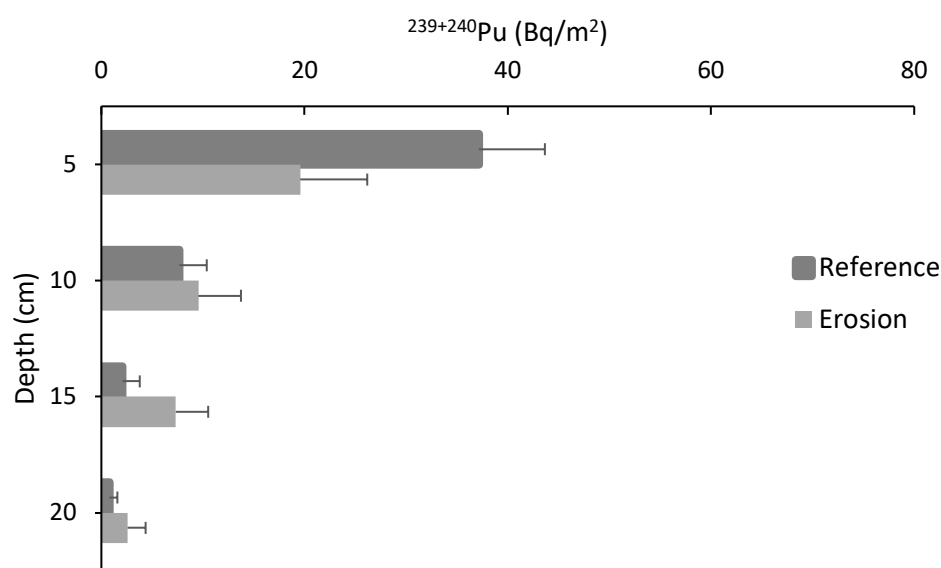
Figure 20: $^{239+240}$Pu activity with depth for samples of profile 173.

Results

The $^{239+240}$Pu activity for both sites in profile 177 decreases with depth, whereby the $^{239+240}$Pu activity for the erosion site is slightly higher in each sampling layer (Figure 21). Therefore, also the inventory of the erosion site is higher to the reference site with 56.55 ± 13.08 Bq/m² and 36.45 ± Bq/m², respectively. The calculated erosion rates range between 0.79 t/ha/year to 1.25 t/ha/year.

Table 6: $^{239+240}$Pu activities (Bq/m²) at profile 177 for each sample. Ref = reference, E = erosion and TUR = tree uprooting.

Sample site Profile 177	0 – 5 cm	5 – 10 cm	10 – 15 cm	15 – 20 cm	Inventory (Bq/m²)
Ref 1	31.48	2.04	3.10	0.85	37.47
Ref 2	45.29	3.17	0.41	0.12	48.99
Ref 3	21.87	1.93	1.32	0.32	25.44
Ref 4	27.51	1.57	1.50	0.66	31.24
E 1	38.75	11.50	1.77	1.14	53.16
E 2	63.36	6.01	1.29	0.44	71.10
E 3	19.82	5.74	3.59	3.94	33.08
E 4	58.61	2.62	1.07	2.38	64.69
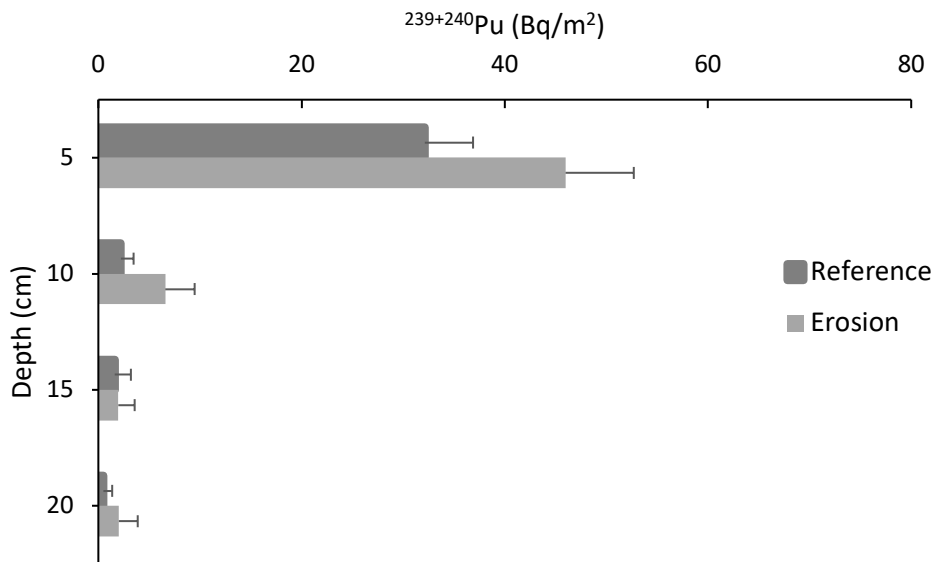
Figure 21: $^{239+240}$Pu activity with depth for samples of profile 177.

3.4. Aggregate Stability

The MWD values did not vary greatly and were for all three profiles approximately 2 (Table 8). Based on Le Bissonnais (1996) values over 1.3 value/mm have high stability or are even very stable over 2 (Table 7).

*Table 7: Categories of aggregate stability based on Le Bissonnais (1996). * = classes of our measured samples.*

MWD (value/mm)	Stability
< 0.4	Very unstable
0.4 – 0.8	Unstable
0.8 – 1.3	Medium
1.3 – 2.0 *	Stable
> 2.0 *	Very stable

The predicted MWD values, using the equation of Chenu et al. (2011), differ slightly to the calculated MWD values based on the fast wetting method. The highest difference is found in profile 177 which can be explained by the high C content in Ah horizon in the profile. Comparing the MWD values to the classes of Le Bissonnais it can be said that the aggregates around the profiles are stable to very stable.

Table 8: Results for calculated and estimated MWD.

Profile	MWD Calculated using Le Bissonnais, 1996	MWD based on Chenu et al., 2011 with parameters			
		MWD	C in Ah	Clay in Ah	Environmental factor (forest)
61	2.04	2.37	5.95	0	0.34
173	1.99	2.32	5.8	0	0.34
177	2.06	5.68	15.66	0	0.34

The particle size distribution is very similar between the profiles (Figure 22). The highest amount of particles is in profile 61 over a diameter of 5 mm. In general, the profiles show a typical decreasing trend of particle sizes. Only the profile 177 has exceptional many particles in size class > 1 mm.

Mean particle size distribution
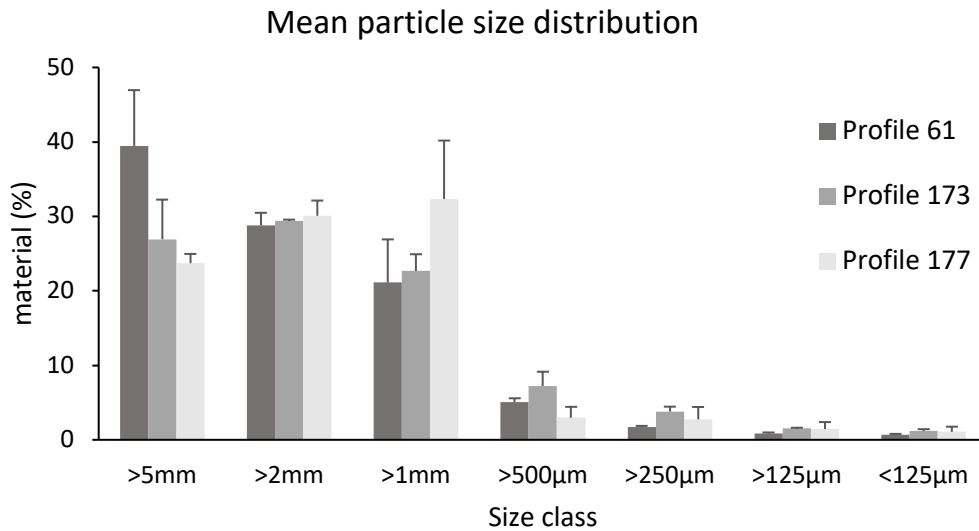
Figure 22: Distribution of particle size into the sieve classes after sieving in percent.

3.5. Soil Properties

Acidity (pH), grain size distribution and elemental composition of the soils are described in this chapter. The Laboratory of K-GEO measured these parameters. These parameters were taken from a previous soil profile excavation in 2014. All predefined horizons were sampled and analysed for our measurements of [10]Be, XRF, C and N content. We sampled only the main horizons because of time and financial limitation as well as a minimum sampling volume needed for the measurements. Not all defined horizons were thick enough to sample enough material for analysis. That is why the results by the Laboratory of K-GEO have more data points compared to our profile samples taken in the field.

3.5.1. pH

The pH of profile 61 and profile 177 are similar (Figure 23). It ranges from 3.1 to 4.3. Both profiles have low pH at the surface with increasing trend to a depth of 30 cm. Below a depth of 30 cm, the pH is almost stagnant. The pH of profile 173 starts low with 2.7. The maximum of 4.2 is at a depth of 78 cm in horizon Bs2 where it decreases with depth.
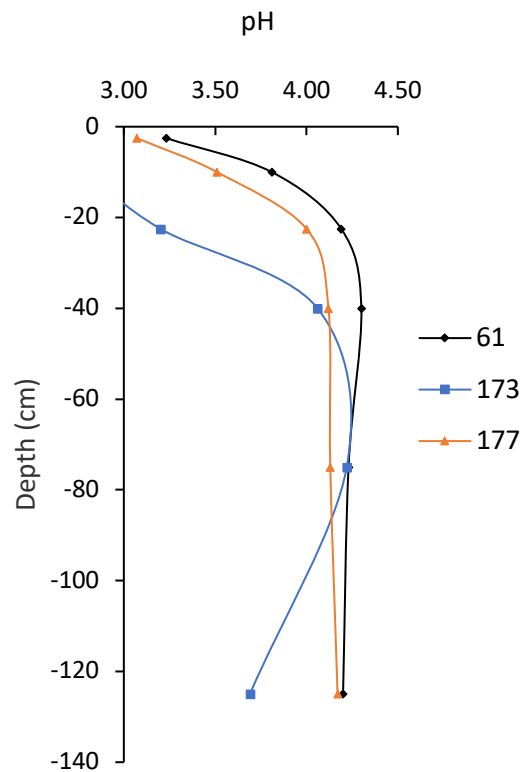
Figure 23: pH of all three profiles measured by the Laboratory of Morava.

3.5.2. Grain Size
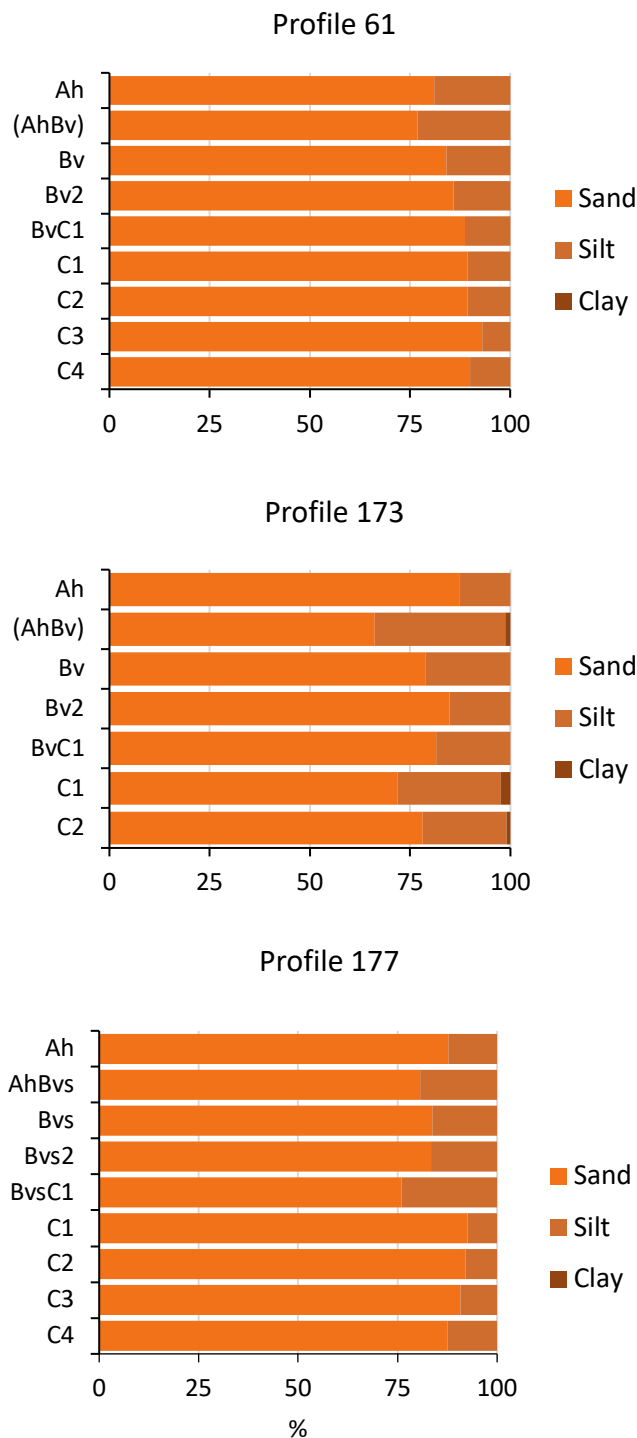
Figure 24: Grain size distribution in percent for each horizon measured by the Laboratory of K-GEO.

The grain size distribution was measured by the Laboratory of K-GEO with the Casagrande method. All three profiles have a high sand content (Figure 24). In profile 61 the grain size increases slightly with increasing depth from 80 to 90% sand content. In profile 61 and 177, no clay was detected in the whole profile. In profile 173, a low clay content was detected in the E, BsC1 and C2 horizon (0.9 – 2.3 %). The profile 173 does not show a size trend. The grain size differs through the horizon whereas sand content is lowest in horizon AhBv and C1. The profile 177 shows two decreasing trends of sand content. From horizon Ah to BvsC1 the sand content decrease. In horizon C1 the highest sand content was measured after which it decreases again with depth.

The results measured by the Laboratory of K-GEO with mostly 0 % clay in all three profiles were surprising. In each profile, one horizon was measured again in Zurich. These results should be used as cross-check of the data. In Figure 25 each measurement is plotted for the remeasured horizon of the specific profile. Three different horizons with different depth and different organic C were selected for the remeasurement. In all remeasured results in Zurich, we could detect clay content between 26 to 4% with highest difference in profile 61 AhBv horizon and lowest in profile 177 Bvs2 horizon. In accordance with higher clay content, the sand content decreases.
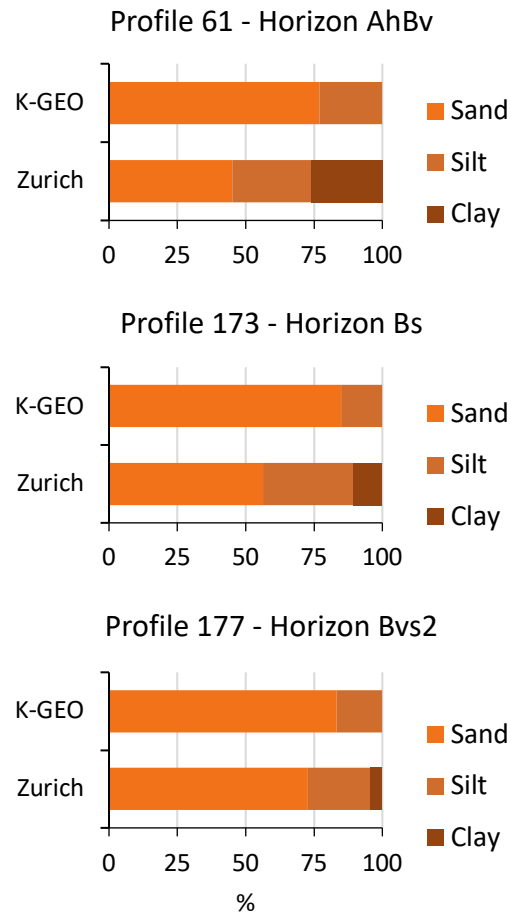
Figure 25: Comparison of grain size distribution measured by the Laboratory of K-GEO and as a control in Zurich. One horizon for each profile was remeasured.

3.5.3. Elemental Composition

The Laboratory of Morava measured the elemental composition of the amorphous and crystalline forms. The concentration of elements in crystalline forms is the difference between the dithionite and the oxalate extraction. Both elemental compositions are distributed homogeneously. The distributions fit typically to the site-specific soil types, for example, the Fe accumulation in the E horizon in the Podzol (Figure 26; profile 173).

Profile 61

Profile 173

Profile 177
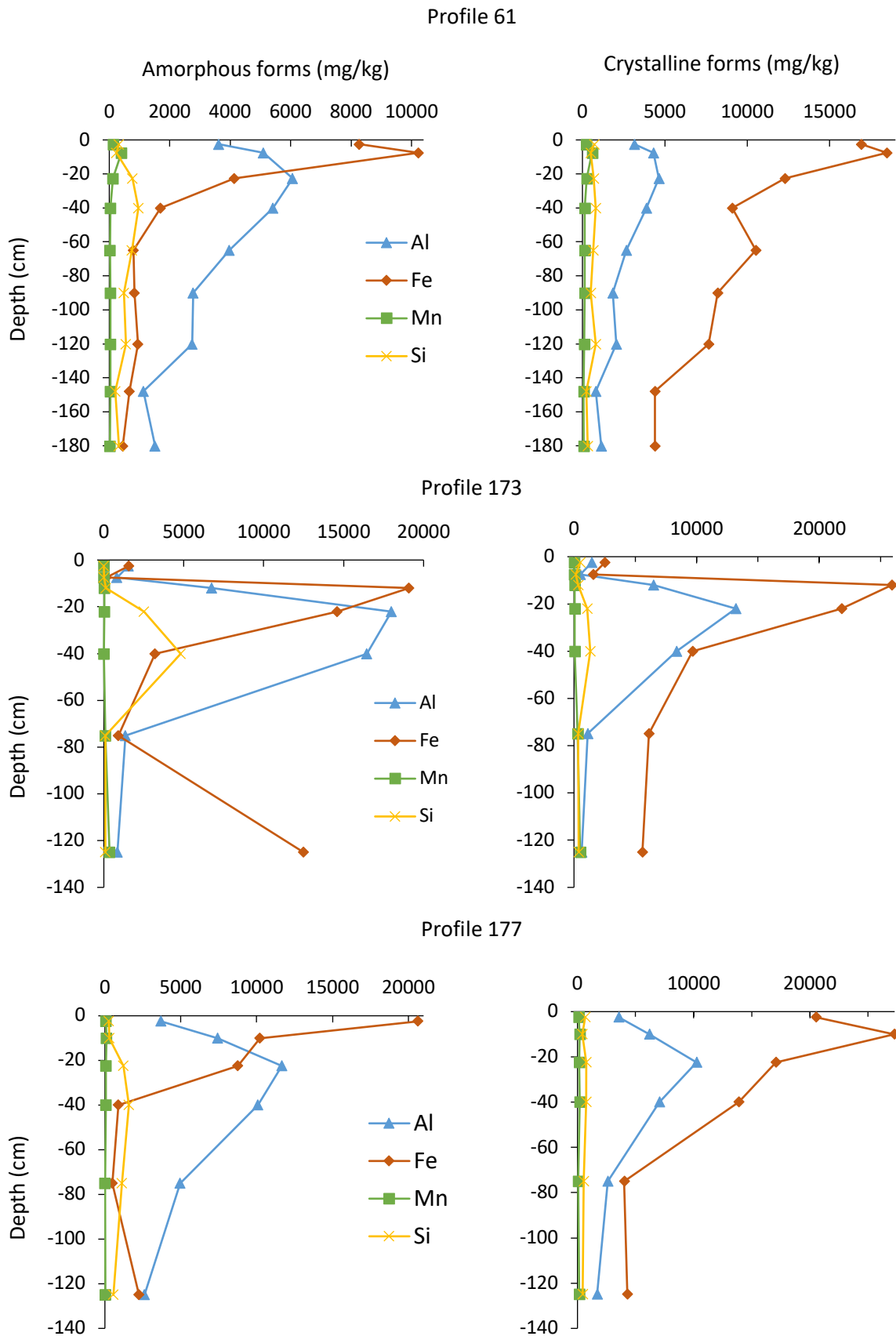
Figure 26: Element composition in percent measured by the Laboratory of Morava in the amorphous (left side) and crystalline form (right side) in percent. Crystalline form is the difference between dithionite and oxalate extraction.

Organic C varies between 1 and 8 % in the first horizon of the profiles and continuously decreases with an exception in profile 173 at the depth between 10 to 20 cm (Figure 27).
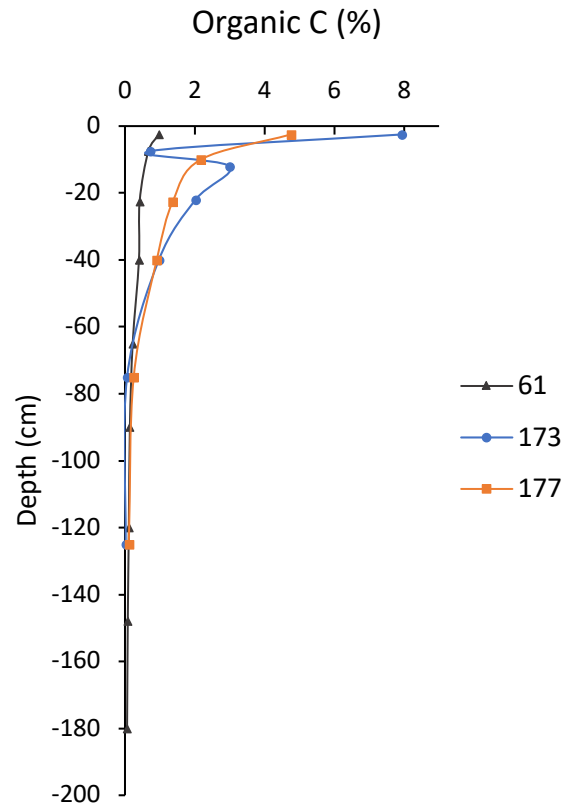
Figure 27: Organic C for all three profiles measured at the Laboratory of Morava.

3.5.4. Geochemistry (XRF)

Also, the elements measured with the XRF are distributed homogeneously. Only the first value for Fe in profile 173 is very low with 0.8 % (Figure 28).
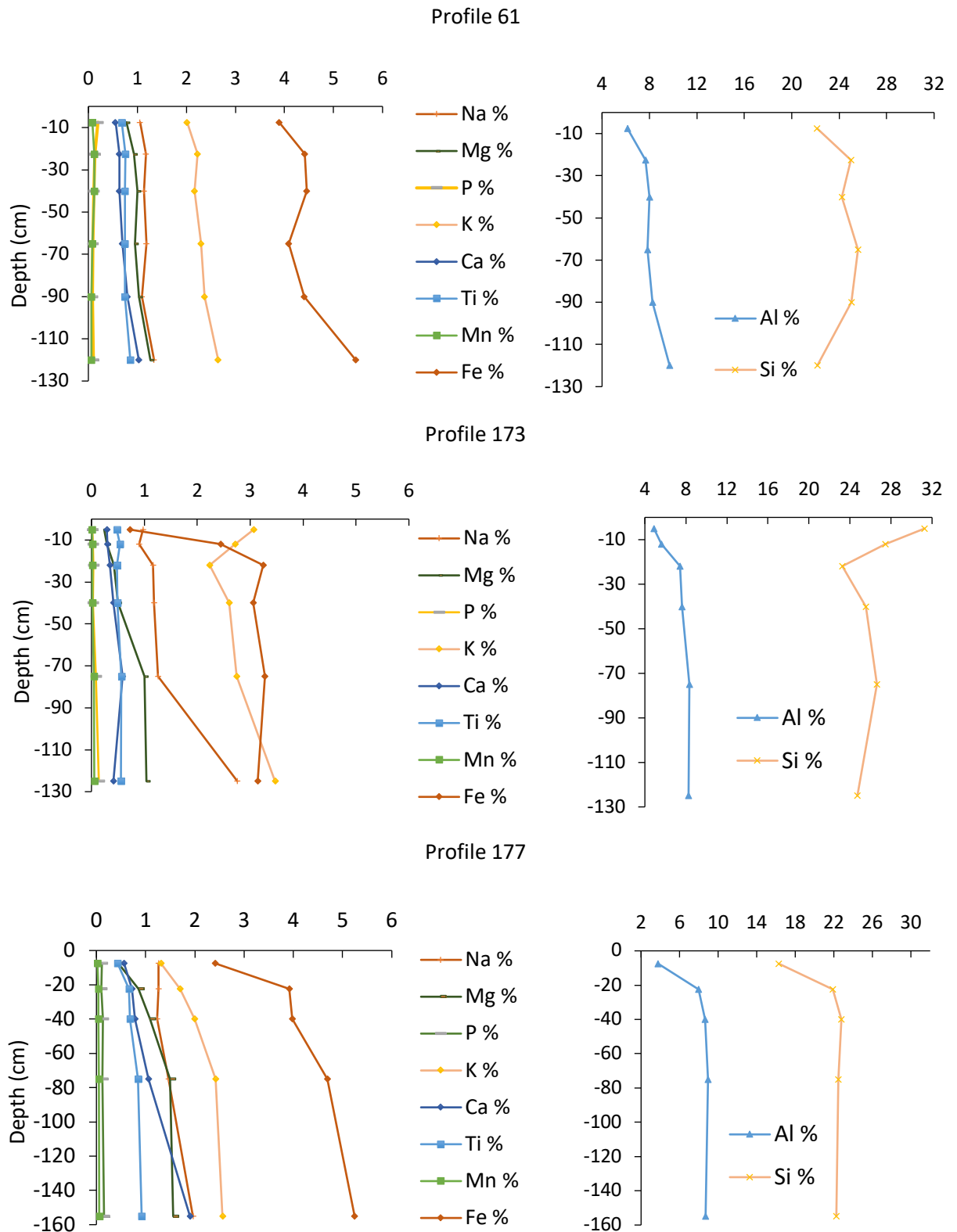
Figure 28: Geochemistry (XRF) element composition in percent measured in Zurich.

3.5.5. Stable Carbon Isotopes

In Figure 29 the C/N ratio and the C content are shown. The C content of the profile 61 decreases with depth from 5.95 – 0.36 %. The C/N ratio in the upper horizon is approximately 14.5. In the horizon C1, the ratio shows an increase to a peak of 18.8 and decreases at the horizon C2 back to 15. In profile 173 the C content stays constant almost for the first 20 cm. Afterwards, it decreases almost to zero at a depth of 80 cm. The C/N ratio of profile 173 shows a peak at horizon Bs2 with 31, decreases to a minimum of 16 and increases again in the C2 horizon. In profile 177 the trend of C content is similar to the profile 61 but has higher concentrations in the first 40 cm. The C/N ratio of profile 177 increases at horizon Bvs2, decreases at horizon BvsC1 and has a maximum of 25 in the horizon C2.
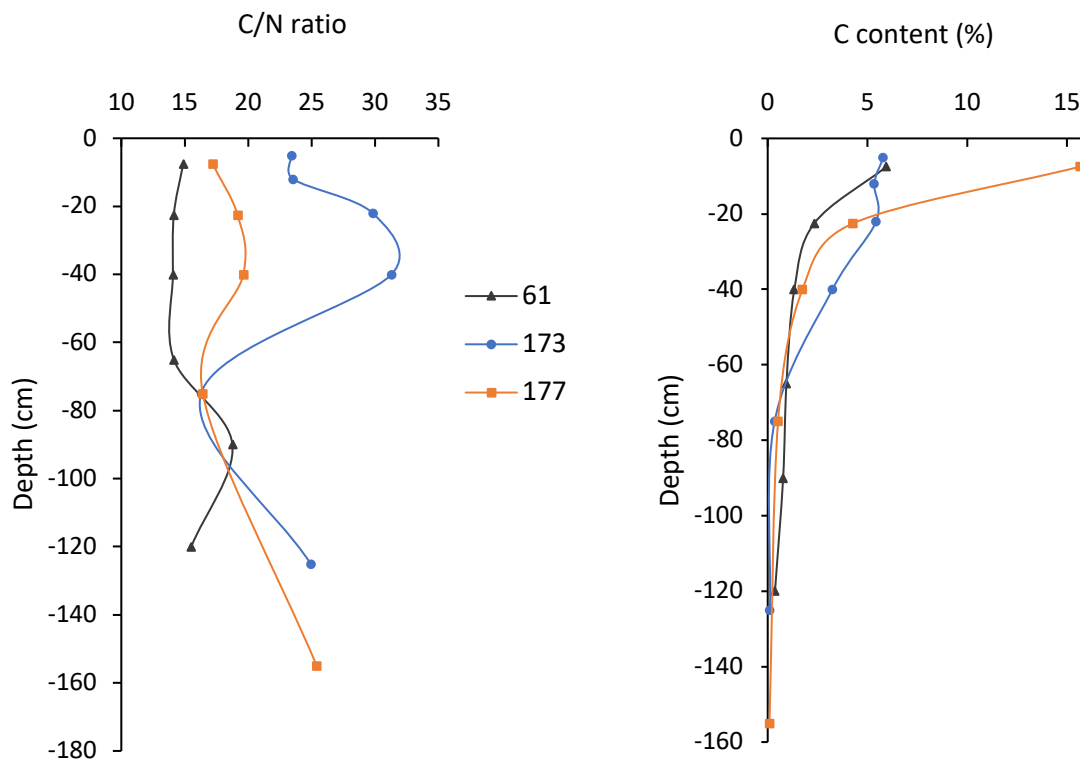
Figure 29: C/N ratio and total C content measured with the IRMS in Zurich.
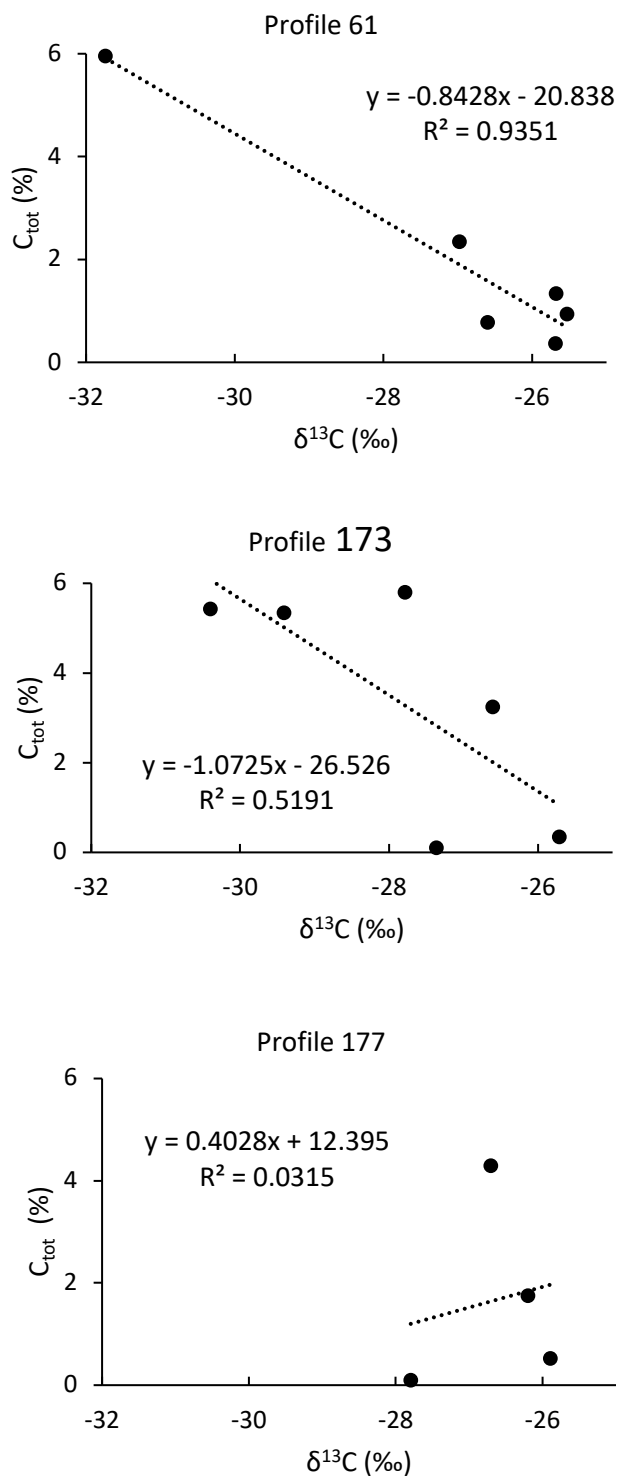
Figure 30: Correlation between the total C content and the isotope signature $\delta^{13}C$.

The $\delta^{13}C$ measurements and the total carbon content (C_{tot}) were measured in Zurich from same samples with the IRMS method. Therefore, they can be compared to each other. In Figure 30, the C_{tot} content is plotted against the $\delta^{13}C$ for each profile. The negative linear regression indicates an indirect correlation between the C_{tot} and the isotope signature $\delta^{13}C$. High C_{tot} values correlate with more negative $\delta^{13}C$ values. In profile 61 highest correlation with R^2 = 0.94 could be detected. The profile 173 has a smaller correlation with R^2 = 0.52. In profile 177 we could not detect a correlation (R^2 = 0.03).

4. Discussion

4.1. Soil Properties

Soil properties can be used to indicate soil formation processes, disturbances and local variations. Consequently, their results are used as additional information to characterise processes in the soil profiles. We estimate undisturbed soil profiles. Hence also undisturbed soil properties.

In all profiles, the soil properties follow average values according to their soil type. The eluviation horizon in profiles 173 and 177 can be discerned with the elemental composition. The pH shows in general, an increasing trend with soil depth and an average around 4. Acidic conditions are characteristic for forest sites.

The typical trajectory of soil development in such environments is a prograding transformation of Cambisol to Podzol soil types (Stahr et al., 2012). Profile 61 that is classified as a Cambisol show first signs of podzolization. It therefore follows the expected soil sequence.

The grain size distribution (< 2 mm) of some selected samples were remeasured in Zurich because the original data did not appear to be meaningful. In all three remeasured samples a clay content of 4 – 26 % was detected. The closer the horizon to the surface and therefore the higher the organic matter content, the higher was the difference between the measurements from the Laboratory of K-GEO and Zurich. We have to assume that organic matter was not destroyed prior to the analyses in the Laboratory of K-GEO. The usage of the grain size distribution data is therefore strongly limited. It can be assumed that the clay content is not 0 % but around 5 – 25 %, which would fit an average clay content in forest soils (Zech et al., 2014). For future analysis, it would be useful to remeasure all horizons of the profiles to get an accurate grain size distribution over the whole profile.

4.2. Qualitative Soil Erosion

The correlation between C content and the isotope $\delta^{13}C$ was performed in several investigations. Zollinger et al. (2015) and Meusburger et al. (2013) described the usage of $\delta^{13}C$ signature to describe soil disturbance patterns. It was also used as an indicator for soil erosion in alpine environment (Schaub and Alewell, 2009).

For profile 61 shows high correlation with $R^2 = 0.9$ indicating stable soil that is not affected by soil erosion. With $R^2 = 0.5$ for profile 173, the correlation is low and indicate possible enhanced soil degradation. No correlation could be found for profile 177 with $R^2 = 0.03$. This low value can be explained by the small number of 4 values and possible disturbances. In the uppermost layer AhBvs, the $\delta^{13}C$ was so low that it could not be detected. Based on these few samples the values

need to be interpreted with caution. Possible explaining processes could be the Podzol distribution, high root activity or soil redistribution. These processes could translocate elements into depth or downslope. Based on the positive value of short-term soil erosion the process of soil redistribution can be neglected as an explanation. The Podzol characteristic and present roots at high depth could be detected in the field. Therefore, these two processes are assumed to be the main influencing factors.

The correlation between the C_{tot} and $\delta^{13}C$ can be used as a qualitative indicator of soil disturbances but cannot be used as a quantitative value of soil redistribution (Meusburger et al., 2013). Based on the values for our profiles we can conclude that profile 61 has a low indication for soil disturbances. The Podzols in profile 173 and 177 indicate enhanced soil degradation or soil disturbances. Because of the small sampling number of n = 6 in profile 61 and 173 and n = 4 in profile 177 the values need to be used with caution.

4.3. Surface Exposure Age

4.3.1. Meteoric ^{10}Be Concentrations

The measured meteoric ^{10}Be concentrations of the three sampled profiles provide long-term soil redistribution rates. Additionally, it gives information about long-term disturbances in the soil profiles. We estimated undisturbed profiles with long soil development and specific characteristics matching their soil type. These assumptions could already be supported by the results discussed above.

Undisturbed soils have the highest ^{10}Be concentration in the upper layer and indicate decreasing trends by depth following the weathering front. Our sampled soil profiles show diverse results. For the soil profile 173 and 177 the estimation of an undisturbed profile can be confirmed. The amount of ^{10}Be indicates typical Podzol characteristics. In both profiles the ^{10}Be concentration in the first two horizons is low, representing the eluvial horizon where the elements were washed-out. Below these upper horizons, the ^{10}Be concentration reaches a maximum and thereafter decreases with depth. These are typical distribution equivalent to Podzol development.
For the profile 61 we expected high concentration in the upper horizons and a decreasing trend with depth. This distribution would be characteristic for a Cambisol. But profile 61 shows a disturbed ^{10}Be concentration curve. It increases until a depth of horizon Bv2 (30 – 50 cm). Afterwards, the concentration shows a zigzag curve with increasing depth. Typically soil profiles after TUR show mixed and contorted horizonation or inverted horizons with little or no mixing in the mound (Schaetzl, 1986). The zigzag curve shows a similar pattern like the described TUR disturbed profiles from Schaetzl.

Discussion

Comparing the [10]Be concentration with other depth distributions showed no correlation. Neither Pu or C content nor elemental composition shows a mixing or zigzag curve with depth. Their distributions are matching typical Cambisol characteristics. The results of the soil properties can verify our assumption of an undisturbed profile. Also, the results of [10]Be concentration in profile 173 and 177 and the field observation where no tree uprooting microrelief or any other disturbance could also verify this hypothesis. The results of [10]Be concentration in profile 61 reject our hypothesis.

The longevity of tree uprooting microreliefs ranges from 5 to 2420 years depending on climatic conditions and soil characteristics (Samonil et al., 2010a). Based on the undisturbed short-term results mentioned above and the field observation it can be assumed that the profile was influenced by a tree uprooting at least over a 100 years ago.

During our field trip further soil samples were taken in the first 50 cm of the soil profiles to detect the age of quartz minerals with the in situ [10]Be approach. Dr. Kevin Norton measured the results at the University of Wellington (New Zealand). Unfortunately, the samples were not measured yet and won't be until the end of this master thesis. Nonetheless, they could support the idea of a very old tree uprooting at profile 61. For the future usage of the data, they could give crucial additional knowledge and need to be taken into account.

This summer (2018) further sampling was undertaken in the forest reserve Boubin. It is also a forest site located in the Czech Republic with many tree uprootings. These two additional profiles (in situ and meteoric [10]Be approach) will provide further information. With this data a better understanding of TUR is expected.

4.3.2. Soil Age

The calculated exposure ages of the three profiles give an approximate time range based on the scenario calculation. The hypothesis that the soil is very old because it was not glaciated during the last glacial maximum will be discussed in this chapter.

Table 9: Summary of the age ranges calculated from the scenario calculation of each profile.

	Profile 61	Profile 173	Profile 177
No erosion	44 – 90 ka	23 – 46 ka	34 – 50 ka
0.3 t/ha/year	74 – 210 ka	25 – 55 ka	40 – 85 ka
1 t/ha/year		29 – 71 ka	

Table 9 summarizes the age range of all three profiles. Figure 31 summarizes the different stratigraphic times together with the estimated ages of the soil profiles as well as the age of the tor and the rock samples located in old TUR.

Profile 61 is the oldest soil with starting of the soil development during the middle to late Pleistocene (780 – 11.7 ka). More precisely during the late Riss stage which occurred between 128 to 350 ka in the Alps. It fits the late Saalian stage in northwest Europe (MIS 5e – 10). Profile 173 and 177 are younger and developed during the late Pleistocene in the Würmian glaciation stage (MIS 5 – 2). The Würm glaciation stage is equivalent to the Weichselian stage in northwest Europe from 115 – 11.7 ka. Glacial activity and cold climate conditions characterise this time range. The Eemian (MIS 5c – 5e) is an interglacial period between the Riss and the Würm with higher temperatures (Schaetzl and Thompson, 2015).
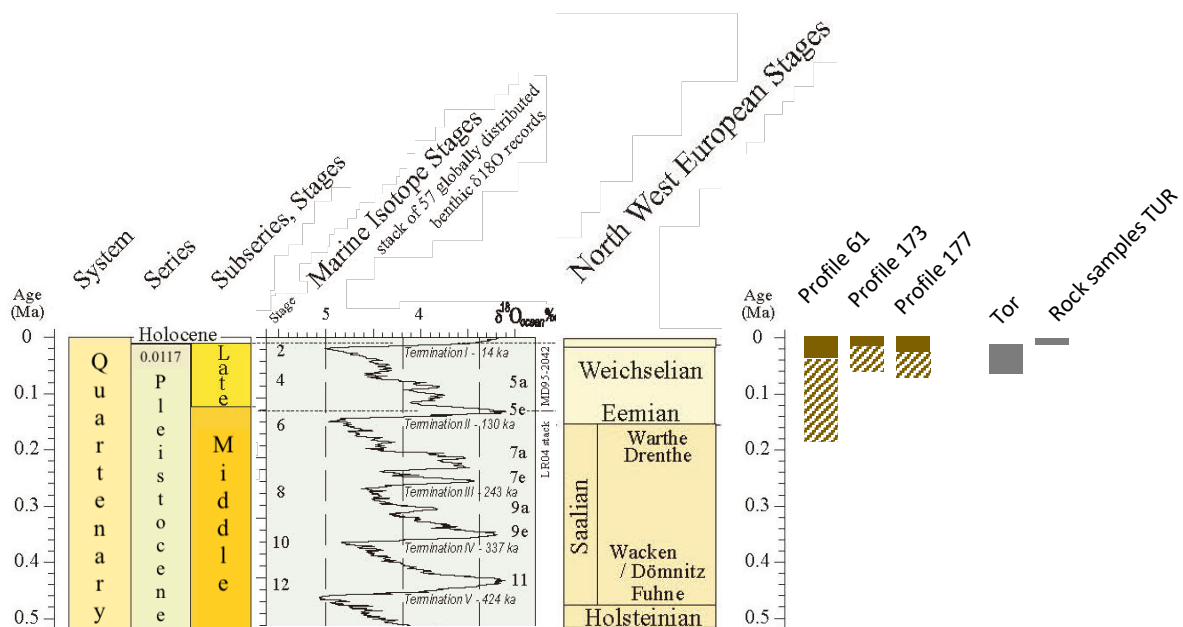
Figure 31: Chronostratigraphic correlation table for Europe sample ages. The brown colored bars are representing the soil profiles measured by meteoric ${}^{10}Be$. The grey bars represent rock samples (tor and all rock samples uplifted by TUR) measured by in situ ${}^{10}Be$. Filled brown bar = Minimum age, lined brown bar = estimated time range until maximum age, grey bar = time range of minimum to maximum calculated age. (ICS, 2016)

The primary ecological zone during the Pleistocene in Europe was shrub-tundra and changed over time to boreal forest. Firstly, the landscape was covered by grassland with time shrubs and trees with a maximal height of 3 – 4 meters. Due to the cold climate, there was low precipitation rates and deep seasonal frost. The last glacial maximum during the Würm did not reach Zofin, but the area was covered by continuous permafrost disturbing the soil (French, 2017; Walling and He, 1999). Due to climate conditions, most soils have formed during the Pleistocene like our soils in the Zofin forest (Schaetzl and Thompson, 2015).

Under the soil development aspect, a Cambisol is normally stratigraphically younger than a Podzol. Our results detected the contrary. The Cambisol is the oldest and Podzols the younger soils. This result suggests that different processes took place in the Cambisol than in the Podzols. Due to burial, erosion or shifts in pedogenic processes soils can form several times and can have more than one time$_{zero}$, where the pedogenic processes start (Schaetzl and Thompson, 2015). This mutability of time$_{zero}$ could be one possible explanation for our oldest soil that is classified as Cambisol. The present Cambisol is the developed soil during the second time$_{zero}$. But the measured soil age of profile 61 is the soil age reaching until the first time$_{zero}$ and initial soil development. Therefore, the initial development of the soil at profile 61 is starting 210 ka ago the present Cambisol approximately around the late Pleistocene were also the Podzols were formed.

Regardless of the soil development, the speed of development can also vary under local conditions. Another explanation of the different ages is associated with the speed of soil processes at the local conditions. At the slope of profile 173 (bottom) and 177 (top) the influence of water might have been higher and sped up the processes and therefore the soil development.

4.3.3. Comparison of the In Situ [10]Be Measurements

For the in situ [10]Be different rocks and one tor were sampled. With help of the tor surface lowering and consequently long-term erosion rates should be calculated. The rocks were all located in old tree uprooting locations where the tree trunk already had been rotten. These samples were corrected by the measured subsurface rock sample that should indicate the amount of preexposure. By sampling these rocks, we tried to date the tree uprootings.

With 66.7 ka the tor is in the time range of our soil profiles. Like suggested the tor is the oldest measured age with help of the in situ [10]Be. The calculated long-term erosion rate based on the three tor samplings was 0.3 t/ha/year. This is a reasonable value that is similar to other erosion rates in a forest (Morgan, 1999; Pieri, 1992). The value is used as erosion rate assumption for the soil age calculation for the meteoric [10]Be mentioned above.

The ages of the rock samples are 20 ka, 8 ka, 10 ka and 13 ka. They can be assigned to the end of the Holocene (present – 11.7 ka). Like mentioned above the vegetation was probably shrub-tundra influenced by permafrost during the Pleistocene. Considering the climatic and vegetation factor, the age of 20 ka is very unlikely because no trees were present at that time. The other samples with ages between 8 to 13 ka are reasonable. With increasing temperature, the number of trees increased.

These ages support the assumption that TUR are important processes that have existed for a long-time in this area (Samonil et al., 2009; Schaetzl and Follmer, 1990).

One reason for the unrealistic age of 20 ka could be a higher amount of preexposure. We just had one rock to estimate the preexposure for all samples. More subsurface rock samples at different depth could give a better overview about possible preexposure. The sampling of one additional subsurface rock sample and one rock at the surface of an old TUR was already taken this summer. During that field trip two other tors, as well as two different heights of the same tor that we looked at this thesis, were sampled. If the average preexposure would be higher, the age of our rocks would consequently be younger. Nevertheless, it can be assumed that the time range of 8 – 13 ka is reasonable.

The approach of measuring old TUR with help of in situ ^{10}Be was done the first time in this thesis. The results demonstrate that it is a possible approach when other methods are not possible anymore.

4.4. Fallout Radionuclides

4.4.1. $^{239+240}$Pu Inventory

With help of the $^{239+240}$Pu activity, short-term soil redistribution can be calculated since it was globally distributed through nuclear weapon testing in the 50s and 60s (with a peak in 1963/64). It is accumulating at the soil surface through precipitation and fixed to organic matter. As organic matter has the highest concentration at the surface and decreases with depth, the same trends are expected for $^{239+240}$Pu activity. Lower Pu concentrations are detectable on erosive sites where the upper soil particles are removed due to erosion by water, wind or snow (Zollinger et al., 2015).

Investigations in grassland or forest ecosystems detected a relationship between organic matter concentration and $^{239+240}$Pu activity (Bunzl et al., 1998; Komosa, 1999; Xu et al., 2013). In our results, similar trends could be measured with the exception of profile 173. In this profile, a clear Podzol distribution could be detected in the organic matter but not in the $^{239+240}$Pu activity. The $^{239+240}$Pu activity of all three profiles shows a generally decreasing trend. The highest change in the $^{239+240}$Pu activity could always be detected in the first 5 – 10 cm. Bunzl et al. (1998) measured the samples at a depth 0 – 2, 2 – 5, 5 – 10 and 10 – 20 cm with the highest $^{239+240}$Pu difference between the first two sampling layers. Due to accumulation process mentioned above, it is reasonable that the highest difference in the $^{239+240}$Pu activity is located in the first few centimetres.

Zollinger et al. (2017) and Alewell et al. (2013) focused on $^{239+240}$Pu activity in alpine environment. The research for grassland and forest environment was conducted by Bunzl et al. (1998) and Xu et al. (2013). The inventories measured in grassland and forest environment are similar to the results of this thesis with 35.9 to 75.4 Bq/m² and 36.5 to 77.8 Bq/m², respectively. The inventories

in the alpine environment are higher with a range of 92 - 246 Bq/m^2 (Alewell et al., 2013; Zollinger et al., 2017). Vegetation cover reduces the chance of precipitation rates reaching the soil surface. Additional processes such as root uptake can alter the $^{239+240}$Pu activity in the soil (Zollinger et al., 2015). In the alpine environment vegetation cover is rare and consequently higher $^{239+240}$Pu activity occurs in the soil.

4.4.2. Erosion Rates

The total inventory reduction was highest at the TUR site at profile 61 with 24 %. The erosion sites of profile 61 and 173 were very similar with 22 % and 18 %. The increase in 55 %, instead of an expected decrease, of the inventory at the site 177 was surprising. The changes in inventories were used to calculate the erosion rates.

When looking at the erosion rates and the inventories, similar patterns can be detected. For the alpine environment erosion rates of 8.3 t/ha/year were measured (Alewell et al., 2013). In our study, we measured soil erosion from 0.83 to 1.36 t/ha/year. The highest erosion occurs at the mound of the TUR were fresh material deposited, and the slope was steepest. At profile 177 we could not measure erosion but deposition of 1.09 t/ha/year. We did not expect deposition at this site because it is at the steepest slope of our sampling with a 20° dip. In addition to the location of the profile, erosion rates in a forest are in general diverse and take place step-wise and not linearly. *The Pu sampling at profile 177 could be located at a side where short-term deposition occurred. The material would erode probably in a next step downslope.* Furthermore, small disturbances induced by animals cannot be excluded with certainty. Such minor variations might influence the $^{239+240}$Pu activity and therefore also the erosion rate at profile 177. Apart from these processes, a clear explanation of the different results of profile 177 could not be found.

Generally, it can be summarised that the erosion rates in the Zofin forest are low. The vegetation stabilises the soil surface and reduces soil erosion. Therefore, the hypothesis that soil redistribution is close to zero in forested areas could be sustained against our assumptions.

Three different models were used in this thesis. The different values were very similar with high correlation between all models (R^2 = 0.95 – 0.99, Figure 32). Meusburger et al. (2016) compared the models IM and MODERN with each other.

They found high correlations, but the erosion rates based on the IM were twice as high than the one from MODERN. Our values for the soil redistribution were very similar and did not vary like in Meusburger et al. (2016). The results of the models vary if the sampling site is cultivated, while we couldn't measure differences in Zofin forest. Since we were interested exclusively on forest sites in this study, we cannot qualify the difference between the models under cultivated conditions.

By measuring the Pu concentration, we were able to calculate low erosion rates in the Zofin forest. Additionally, we could show that the erosion rate located on the mound was highest in our samples. This result supports the idea of higher erosion rates at mounds compared to natural forest relief. To be able to differentiate TUR erosion behaviour further also pits need to be sampled. Two pits and mounds were sampled already in the forest reserve of Boubin. It is located in the Czech Republic like the Zofin forest and has the same climate conditions. The comparison of the two different forest will be a valuable contribution to this topic.

Figure 32: Correlations between erosion rates of the different models that were used in this study: PDM, IM and MODERN.

4.4.3. Comparison of Erosion Rates

The short-term erosion rate covers a time range from 1963 to present, whereas the long-term erosion rates with the ^{10}Be approach can cover periods over millennia. The measured tor could be dated to the Würm period and give approximate erosion rates during that time. Glacial and interglacial phases characterised this climate conditions. Zofin was not covered by glacial but was

influenced by the cold and dry weather conditions. The soil was affected and disturbed by permafrost.

The long-term erosion rates are considerably lower than the short-term erosion rates. As previously mentioned, vegetation cover has an important influence on soil erosion rates. It needs to be considered that with the changing climate from Würm to the Holocene the vegetation changed from grassland to forest. Nevertheless, the short-term erosion is higher compared to the long-term erosion rate. This comparison needs to be used with caution because of too few data points (just one tor sampling).

4.5. Aggregate Stability

With help of the aggregate stability we measured recent soil erosion and complete erosion rates in different time ranges together with the other erosion measurements. As the study area is located at a forest site we expected very high aggregate stability. The high amount of organic matter in the forest assembles stable aggregates that resist erosion processes. Besides organic matter, the aggregate stability is also correlated to the clay content. Both have binding and stabilising characteristics. The results of the grain size distribution have some uncertainties that were discussed in chapter 4.1. Before remeasuring the clay content was 0 %, afterwards we estimate a variance of clay content between 4 to 26 % in our soils. The measured organic matter at all sites is between 1 to 8 %.

Based on the method of Le Bissonnais (1996), the soil aggregates can be classified as stable to very stable. Such aggregate stability has to be expected for forest environments. In addition to the fast wetting method, we calculated the MWD based on Chenu et al. (2011). The MWD's were very similar but showed higher MWD for profile 177. This is due to the very high C content with 15.66 % in the Ah horizon. The difference of the calculated MWD considering the two measured clay contents (0 % or an average of 18 %) is about 1.4. But independent of the clay content or the method that is used for the MWD calculation the aggregate stability is high for all profiles and in the expected stability class.

With help of the wet sieving MWD and the estimated MWD, we could verify our hypothesis. Based on our results it can also be assumed that the high amount of TUR does not influence the aggregate stability at this forest site. With no soil structure, this correlation would be detected.

Principal component analysis (PCA) is a multivariate technique. It is used to identify the linear components within data sets (Field et al., 2012). With the PCA, patterns in data sets can be visualized. We used this qualitative approach to visualize patterns in our data set of soil properties in the soil profiles (Figure 33).
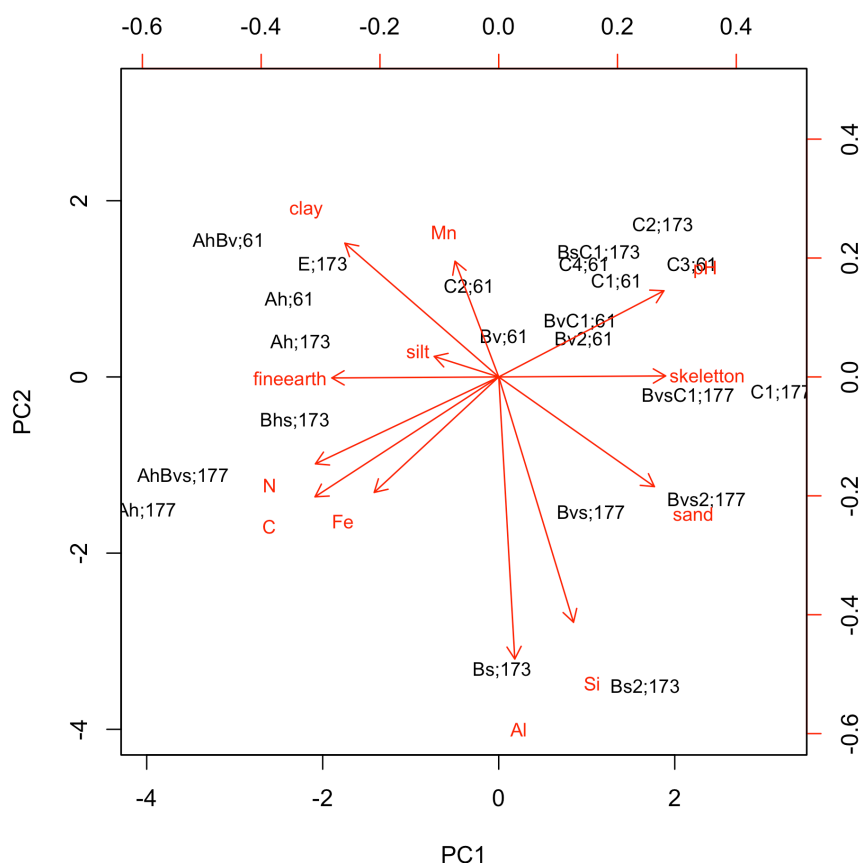
Figure 33: Principal component analysis (PCA) based on soil properties of all three profiles. The amorphous forms were used for the element values (Fe, Mn, Si, Al). The C and N contents are from the IRMS measurement at the Laboratory of Zurich. A clay content of 18 % was estimated for all horizons based on the remeasurement at the Laboratory of Zurich.

The first and second principal component (PC1; PC2) explain 38.5 and 19 % respectively of the total variance. In Figure 33 the distribution of the components is visualized. The distribution of the components is the same for 0 % clay content or the estimated clay content of 18 % (Appendix Figure 1). Their PC1 and PC2 explain with 32.8 and 19 % of the total variance less than with the estimated clay content of 18 %. PC1 was positively correlated with the % of the fine earth, the N and C content as well as the amorphous Fe. In contrast, PC1 was negatively related to % of skeleton and pH. The projection of soil horizons on PCA shows that the PC1 characterise the horizons of profile 61 and 177. The profile 173 is more located in the area of PC2. The positive part of PC2 is characterised by % of clay and silt as well as the amorphous Mn. Negatively it was associated with % of sand, amorphous Si and Al. The distribution of the parameters is reasonable. Silicium is part of sand particles and is therefore located in the same area. Also, N and C, as well as silt and clay are components that are correlated to each other, and thus they are located in the same area.
It can be seen that the different horizons of the profiles are located in the same area, meaning that they have similar characteristics.

5.   Conclusion

We successfully managed to date the surface of the Zofin forest as well as the rocks in old tree uprooting. Additionally, we could detect short and long-term erosion with the help of $^{239+240}$Pu activity and ^{10}Be concentration.

The exposure ages of the soils in the Zofin forest could be measured with meteoric ^{10}Be. The assumption of very old soils could be verified. The different profiles have a soil age reaching early to late Pleistocene. Due to the depth distribution of the ^{10}Be concentration, it can be recorded that profile 61 is located at a site disturbed by tree uprooting. All other profile analysis did not show any disturbance pattern. As a result, it can be assumed that the tree uprooting happened over 100 years ago. The assumption of undisturbed reference profiles can therefore not be verified for all profiles.

The short-term erosion derived from Pu distribution in the forest could be measured. With help of the PDM, IM and the MODERN model the inventory loss of Pu could be converted into soil redistribution rates. Soil erosion as well as soil deposition could be detected. The soil loss of profile 61 and profile 173 is with 18 – 24 % comparable to other researches in the forest. The deposition of 55 % of the inventory at profile 177 is unexpectedly high.

We could compare the short and long-term erosion with each other. The long-term erosion rates were slightly lower than the short-term erosion rates. The lower rates could be located to the cold and dry climate during the Pleistocene.

We could determine the age of a boulder located in an old tree uprooting. With help of one sample measured under the surface, an estimation of pre-exposure could be integrated. The rocks were uplifted to the surface between a period of 8 – 21 ka. The maximum age at the tor could be detected at 67 ka and indicates a long-term erosion rate of 0.3 t/ha/year.

The dating of a very old tree uprooting indicates tree uprootings in the Zofin forest during the beginning of the Holocene.

Our hypothesis of stable soil aggregates in the Zofin forest could be verified. The MWD calculated with the wet-sieving approach as well as the estimation of the MWD indicate stable to very stable aggregates.

References

Alewell, C., Meusburger, K., Juretzko, G., Mabit, L., Ketterer, M.E., 2013. Suitability of 239+240Pu and 137Cs as tracers for soil erosion assessment in mountain grasslands. Chemosphere, 103, 274–280.

Arata, L., Alewell, C., Frenkel, E., A'Campo-Neuen, A., Iurian, A., Ketterer, M.E., Mabit, L., Meusburger, K., 2016. Modelling Deposition and Erosion rates with RadioNuclides (MODERN) - Part 2: A comparison of different models to convert 239+240Pu inventories into soil redistribution rates at unploughed sites. Journal of Environmental Radioactivity, 162–163, 97–106.

Arata, L., Meusburger, K., Bürge, A., Zehringer, M., Ketterer, M.E., Mabit, L., Alewell, C., 2017. Decision support for the selection of reference sites using 137Cs as a soil erosion tracer. Soil, 3, 113–122.

Bunzl, K., Kracke, W., Schimmack, W., Zelles, L., 1998. Forms of Fallout 137Cs and 239+240Pu in Horizons of a Forest Soil Successive. Journal of Environmental Radioactivity, 39, 55–68.

Chenu, C., Abiven, S., Annabi, M., Barray, S., Bertrand, M., Bureau, F., Cosentino, D., Darboux, F., Duval, O., Fourrié, L., Francou, C., Houot, S., Jolivet, C., Laval, K., Le Bissonnais, Y., Lemée, L., Menasseri, S., Pétraud, J.P., Verbèque, B., 2011. Mise au point d'outils de prévision de l'évolution de la stabilité de la structure de sols sous l'effet de la gestion organique des sols. Étude et Gestion des Sols, 18, 161–174.

Chmeleff, J., von Blanckenburg, F., Kossert, K., Jakob, D., 2010. Determination of the10Be half-life by multicollector ICP-MS and liquid scintillation counting. Nuclear Instruments and Methods in Physics Research B, 268, 192–199.

Christl, M., Vockenhuber, C., Kubik, P.W., Wacker, L., Lachner, J., Alfimov, V., Synal, H.A., 2013. The ETH Zurich AMS facilities: Performance parameters and reference materials. Nuclear Instruments and Methods in Physics Research B, 294, 29–38.

Cosmogenic Nuclide Lab, U.W., 2016. CRONUS earth. Cosmic-Ray Produced Nuclide Systematics on Earth Project. [Online] 2016. https://hess.ess.washington.edu/.

Egli, M., Brandová, D., Böhlert, R., Favilli, F., Kubik, P.W., 2010. 10 Be inventories in Alpine soils and their potential for dating land surfaces. Geomorphology, 119, 62–73.

Egli, M., Brandova, D., Röthlisberger, S., Woodhatch, I., Zollinger, B., 2015. Geochronology laboratory methods. University of Zurich.

Field, A., Miles, J., Zoe, F., 2012. Exploratory factor analysis, in: Discovering Statistics Using R. SAGE Publications, 749–811.

Fitton, G., 1997. X-ray fluorescence spectrometry, in: Gill, R. (Ed.), Modern Analytical Geochemistry: An Introduction to Quantitative Chemical Analysis Techniques for Earth,

References

Environmental and Materials Scientists. Routledge, 87–115.

French, H.M., 2017. Periglacial Ecosystems, in: The Periglacial Environment. John Wiley & Sons Ltd, 41–61.

Heyman, B.M., Heyman, J., Fickert, T., Harbor, J.M., 2013. Paleo-climate of the central European uplands during the last glacial maximum based on glacier mass-balance modeling. Quarternary Research, 79, 49–54.

Horiuchi, K., Minoura, K., Kobayashi, K., Nakamura, T., Hatori, S., Matsuzaki, H., Kawai, T., 1999. Last-glacial to post-glacial 10Be fluctuations in a sediment core from the Academician Ridge, Lake Baikal. Geophysical Research Letters, 26, 1047–1050.

Hu, Q.H., Weng, J.Q., Wang, J.S., 2010. Sources of anthropogenic radionuclides in the environment: A review. Journal of Environmental Radioactivity, 101, 426–437.

ICS, 2016. International Comission on Stratigraphy (ICS). Subcomission on Quaternary Stratigraphy (SQS). [Online] 2016. http://www.stratigraphy.org/index.php/ics-chart-timescale.

Kelley, J.M., Bond, L.A., Beasley, T.M., 1999. Global distribution of Pu isotopes and 237Np. Sci. Total Environ., 237/238, 483–500.

Ketterer, M.E., 2015. Standard Operating Procedure for Preparation of Soils and Sediments for 239+240Pu Activity and 240Pu/239Pu Atom Ratio Measurements – Acid Leaching and Quadrupole ICPMS.

Ketterer, M.E., Szechenyi, S.C., 2008. Determination of plutonium and other transuranic elements by inductively coupled plasma mass spectrometry: A historical perspective and new frontiers in the environmental sciences. Spectrochimica Acta - Part B Atomic Spectroscopy, 63, 719–737.

Komosa, A., 1999. Migration of plutonium isotopes in forest soil profiles in Lublin region (Eastern Poland). Journal of Radioanalytical and Nuclear Chemistry, 240, 19–24.

Kooch, Y., Darabi, S.M., Hosseini, S.M., 2015. Effects of Pits and Mounds Following Windthrow Events on Soil Features and Greenhouse Gas Fluxes in a Temperate Forest. Pedosphere, 25, 853–867.

Korschinek, G., Bergmaier, A., Faestermann, T., Gerstmann, U.C., Knie, K., Rugel, G., Wallner, A., Dillmann, I., Dollinger, G., von Gostomski, C.L., Kossert, K., Maiti, M., Poutivtsev, M., Remmert, A., 2010. A new value for the half-life of 10Be by Heavy-Ion Elastic Recoil Detection and liquid scintillation counting. Nuclear Instruments and Methods in Physics Research B, 268, 187–191.

Lal, D., 2001. New Nuclear Methods for Studies of Soil Dynamics Utilizing Cosmic Ray Produced Radionuclides, in: Stott, D.E., Mohtar, R.H., Steinhardt, G.C.(Eds.) Sustaining the Global Farm. 10th International Soil Conservation Organization Meeting, Purdue University and

USDA-ARS National Soil Erosion Research Laboratory. 1044–1052.

Lal, R., Tims, S.G., Fifield, L.K., Wasson, R.J., Howe, D., 2013. Applicability of 239Pu as a tracer for soil erosion in the wet-dry tropics of northern Australia. Nuclear Instruments and Methods in Physics Research B, 294, 577–583.

Le Bissonnais, Y., 1996. Aggregate stability and assessment of soil crustability and erodibility : I. Theory and methodology. European Journal of Soil Science, 47, 425–437.

Maejima, Y., Matsuzaki, H., Nakano, C., 2004. Be concentrations of Red soils in Southwest Japan and its possibility of dating. Nuclear Instruments and Methods in Physics Research B, 223–224, 596–600.

McHargue, L.R., Damon, P.E., 1991. The global beryllium 10 cycle. Reviews of Geophysics, 29, 141–158.

Meusburger, K., Mabit, L., Ketterer, M.E., Park, J.H., Sandor, T., Porto, P., Alewell, C., 2016. A multi-radionuclide approach to evaluate the suitability of 239 + 240Pu as soil erosion tracer. Science of the Total Environment, 566–567, 1489–1499.

Meusburger, K., Mabit, L., Park, J.H., Sandor, T., Alewell, C., 2013. Combined use of stable isotopes and fallout radionuclides as soil erosion indicators in a forested mountain site, South Korea. Biogeosciences, 10, 5627–5638.

Monaghan, M.C., Krishnaswami, S., Turekian, K.K., 1986. The global-average production rate of 10Be. Earth and Planetary Science Letters, 76, 279–287.

Morgan, R.P.C., 1999. Soil Erosion and Conservation, in: Soil Erosion and Conservation. Blackwell Publishing, 45–65.

Nimmo, J.R., Perkiins, K.S., 2002. Aggregate Stability and Size Distribution, in: Dane, J.H., Topp, G.C. (Eds.), Methods of Soil Analysis, Part 4 - Physical Methods. Soil Science Society of America, Madison, Wisconsin, 317–328.

Nishiizumi, K., Imamura, M., Caffee, M.W., Southon, J.R., Finkel, R.C., McAninch, J., 2007. Absolute calibration of10Be AMS standards. Nuclear Instruments and Methods in Physics Research B, 258, 403–413.

Pieri, C.J.M.., 1992. Fertility of soils : a future for farming in the West African savannah. Springer-Verlag, Berlin.

Raaba, G., Scarcigliab, F., Nortonc, K., Dahmsd, D., Brandováa, D., Portesa, R. de C., Christle, M., Kettererf, M.E., Rupplia, A., Eglia, M., 2018. Denudation variability of the sila massif (Italy) from decades to millennia using 10Be and 239+240Pu. Land Degradation & Development, in press.

Samonil, P., Danek, P., Adam, D., Phillips, J.D., 2017a. Breakage or uprooting: How tree death type affects hillslope processes in old-growth temperate forests. Geomorphology, 299, 76–84.

References

Samonil, P., Danek, P., Schaetzl, R.J., Tejnecky, V., Drabek, O., 2017b. Converse pathways of soil evolution caused by tree uprooting: A synthesis from three regions with varying soil formation processes. Catena, 161, 122–136.

Samonil, P., Danek, P., Schaetzl, R.J., Vasickova, I., Valtera, M., 2015. Soil mixing and genesis as affected by tree uprooting in three temperate forests. European Journal of Soil Science, 66, 589–603.

Samonil, P., Kral, K., Douda, J., Sebkova, B., 2008. Variability in forest floor at different spatial scales in a natural forest in the Carpathians: Effect of windthrows and mesorelief. Canadian Journal of Forest Research, 38, 2596–2606.

Samonil, P., Kral, K., Hort, L., 2010a. The role of tree uprooting in soil formation: A critical literature review. Geoderma, 157, 65–79.

Samonil, P., Santolik, L., Svoboda, M., Adam, D., 2009. Dynamics of windthrow events in a natural fir-beech forest in the Carpathian mountains. Forest Ecology and Management, 257, 1148–1156.

Samonil, P., Schaetzl, R.J., Valtera, M., Golias, V., Baldrian, P., Vasickova, I., Adam, D., Janik, D., Hort, L., 2013. Crossdating of disturbances by tree uprooting: Can treethrow microtopography persist for 6000 years? Forest Ecology and Management, 307, 123–135.

Samonil, P., Tejnecky, V., Boruvka, L., Sebkova, B., Janik, D., Sebek, O., 2010b. The role of tree uprooting in Cambisol development. Geoderma, 159, 83–98.

Samonil, P., Valtera, M., Bek, S., Sebkova, B., Vrska, T., Houska, J., 2011. Soil variability through spatial scales in a permanently disturbed natural spruce-fir-beech forest. European Journal of Forest Research, 130, 1075–191.

Samonil, P., Valtera, M., Schaetzl, R.J., Adam, D., Vasickova, I., Danek, P., Janik, D., Tejnecky, V., 2016. Impacts of old, comparatively stable, treethrow microtopography on soils and forest dynamics in the northern hardwoods of Michigan, USA. Catena, 140, 55–65.

Samonil, P., Vasickova, I., Danek, P., Janík, D., Adam, D., 2014. Disturbances can control fine-scale pedodiversity in old-growth forests: Is the soil evolution theory disturbed as well? Biogeosciences, 11, 5889–5905.

Schaetzl, R.J., 1990. Effects of treethrow microtopography on the characteristics and genesis of Spodosols, Michigan, USA. Catena, 17, 111–126.

Schaetzl, R.J., 1986. Complete soil profile inversion by tree uprooting. Physical Geography, 7, 181–189.

Schaetzl, R.J., Follmer, L.R., 1990. Longevity of threethrow microtopography: implications for mass wasting. Geomorphology, 3, 113–123.

Schaetzl, R.J., Thompson, M.L., 2015. Soils: Genesis and Geomorphology, 2nd ed. Cambridge University Press.

Schaub, M., Alewell, C., 2009. Stable carbon isotopes as an indicator for soil degradation in an alpine environment (Urseren Valley, Switzerland). Rapid communications in mass spectrometry : RCM, 23, 1499–1507.

Stahr, K., Kandeler, E., Herrmann, L., Streck, T., 2012. Bodenkunde und Standortlehre, 2nd ed. Eugen Ulmer Stuttgart.

Valtera, M., Schaetzl, R.J., 2017. Pit-mound microrelief in forest soils: Review of implications for water retention and hydrologic modelling. Forest Ecology and Management, 393, 40–51.

Walling, D.E., He, Q., 1999. Improved models for estimating erosion rates from Cesium-137 measurements. Journal of Environmental Quality, 28, 611–622.

Weil, R.R., Brady, N.C., 2017. The Nature and Properties of Soils, 15th ed. Pearson Education Limited.

Willenbring, J.K., von Blanckenburg, F., 2009. Meteoric cosmogenic Beryllium-10 adsorbed to river sediment and soil: Applications for Earth-surface dynamics. Earth Science Reviews, 98, 105–122.

Xu, Y., Qiao, J., Hou, X., Pan, S., 2013. Plutonium in Soils from Northeast China and Its Potential Application for Evaluation of Soil Erosion. Scientific Reports, 3, 3506.

Zapata, F., 2002. Handbook for the Assessment of Soil Erosion and Sedimentation Using Environmental Radionuclides. Kluwer, Dordrecht.

Zech, W., Schad, P., Hintermaier-Erhard, G., 2014. Böden der Welt, 2nd ed. Springer, Spektrum.

Zollinger, B., Alewell, C., Kneisel, C., Brandová, D., Petrillo, M., Plötze, M., Christl, M., Egli, M., 2017. Soil formation and weathering in a permafrost environment of the Swiss Alps: a multi-parameter and non-steady-state approach. Earth Surface Processes and Landforms, 42, 814–835.

Zollinger, B., Alewell, C., Kneisel, C., Meusburger, K., Brandová, D., Kubik, P., Schaller, M., Ketterer, M.E., Egli, M., 2015. The effect of permafrost on time-split soil erosion using radionuclides (137Cs, 239 + 240Pu, meteoric 10Be) and stable isotopes (δ13C) in the eastern Swiss Alps. Permafrost and Periglacial Processes, 3, 189–192.

Appendix
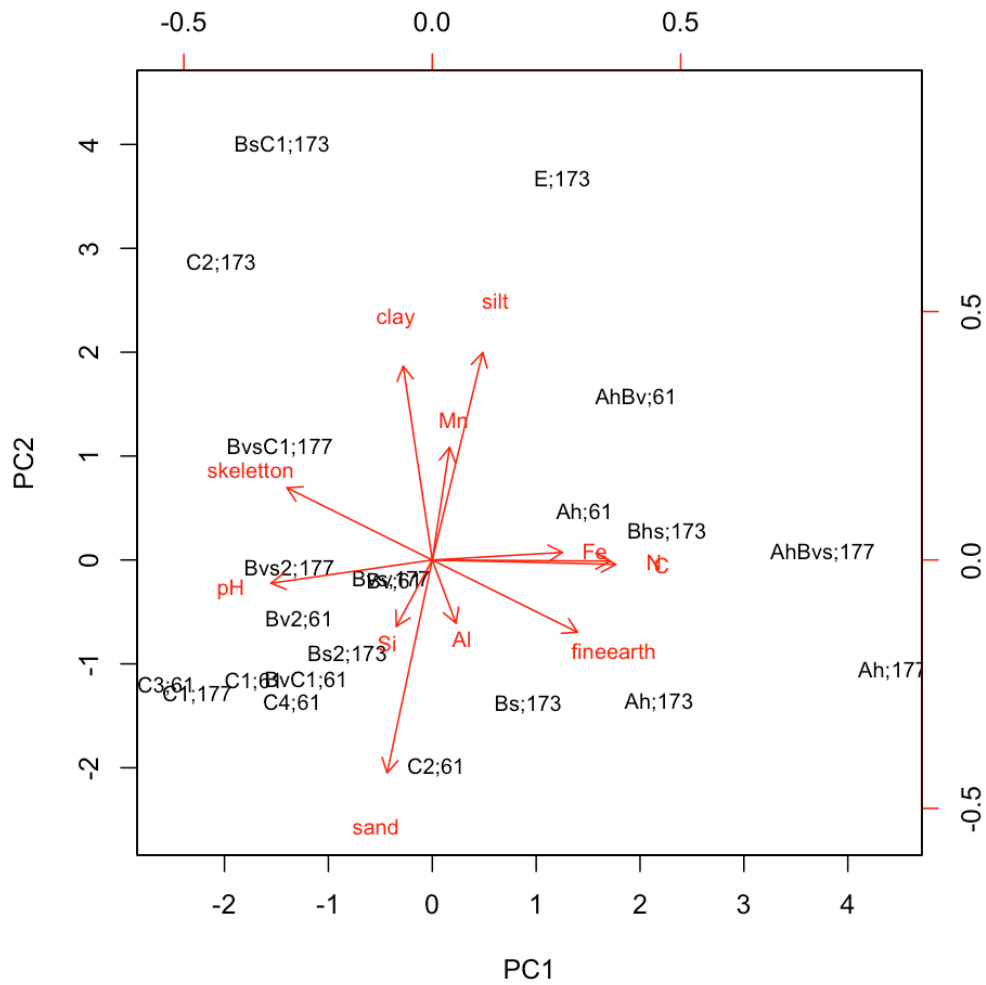
Appendix Figure 1: Principal component analysis (PCA) based on soil properties of all three profiles. The amorphous forms were used for the element values (Fe, Mn, Si, Al). The C and N contents are from the IRMS measurement at the Laboratory of Zurich. The grain size distribution was measured by the Laboratory of K-GEO.

Appendix Table 1: Soil properties measured by the Laboratory of Morava.

Profile	Soil horizon	Depth (cm)	Labile forms Al	Fe	Mn	Si	Amorphous forms Al	Fe	Mn	Si	Crystalline forms Al	Fe	Mn	Si	pH H$_2$O	N$_{tot}$ (%)	C$_{ox}$ (%)
			(mg/kg)				(mg/kg)				(mg/kg)						
61	Ah	5	647	27.8	14.3	14.6	3630	8273	138	311.9	3143	16936	232	700.5	4.03	0.40	6.97
	(AhBv)	15	530	5.18	9.72	16.4	5108	10226	401	237.2	4319	18476	580	491.8	4.46	0.23	3.70
	Bv	30	211	4.20	2.74	21.6	6070	4141	126	766.0	4638	12297	247	673.0	4.84	0.10	1.79
	Bv2	50	145	4.00	1.41	21.7	5418	1690	42.1	962.0	3895	9100	122	792.5	4.94	0.07	1.24
	BvC1	80	146	3.89	1.92	23.3	3968	803	24.5	750.7	2663	10511	136	650.0	4.91	0.05	0.85
	C1	110	140	3.93	1.29	23.4	2780	826	29.4	489.3	1852	8213	125	513.5	5.40	0.03	0.71
	C2	140	124	0.92	1.34	23.3	2750	952	33.9	550.0	2070	7670	106	808.0	5.20	0.04	0.66
	C3	160	96.4	1.07	1.09	17.7	1130	669	37.9	198.0	811	4400	63.3	237.0	5.10	0.03	0.49
	C4	200	63.7	1.04	2.44	21.2	1510	446	25.4	326.0	1150	4400	67.8	323.0	5.20	0.04	0.65
173	Ah	5	255	43.3	3.07	13.4	1552	1584	11.0	15.9	1439	2528	15.7	503.5	3.49	1.31	21.31
	E	10	224	11.0	0.56	6.8	832	162	7.20	10.0	517	1551	16.4	143.7	3.77	0.14	4.85
	Bhs	14	959	107	0.57	15.0	6749	19097	17.6	140.9	6459	25921	36.4	341.6	3.91	0.48	8.44
	Bs	30	343	9.20	0.29	43.6	17993	14591	20.3	2518.0	13186	21825	60.5	1094.5	4.55	0.10	4.11
	Bs2	50	175	5.17	0.24	49.9	16453	3200	11.7	4809.0	8343	9687	61.8	1328.0	4.70	0.08	2.35
	BsC1	100	414	3.71	2.14	15.0	1345	909	108	92.4	1100	6100	283	351.7	4.82	0.03	1.41
	C2	150	47.9	3.31	5.55	19.1	849	12510	356	95.8	621	5585	497	388.7	5.59	0.02	0.91

Appendix

Profile	Soil horizon	Depth (cm)	Labile forms				Amorphous forms				Crystalline forms				pH H₂O	N_tot (%)	C_ox (%)
			Al	Fe	Mn	Si	Al	Fe	Mn	Si	Al	Fe	Mn	Si			
			(mg/kg)				(mg/kg)				(mg/kg)						
177	Ah	5	556	77.8	5.52	23.6	3701	20625	62.6	256.3	3538	20515	102	647.0	3.80	0.76	10.23
	AhBvs	15	587	14.4	4.46	19.3	7440	10202	108	304.3	6176	27251	168	417.2	4.25	0.30	5.26
	Bvs	30	331	4.73	0.63	32.8	11660	8776	65.3	1226.0	10249	17061	152	757.0	4.61	0.13	3.25
	Bvs2	50	261	4.44	0.60	36.8	10088	890	65.5	1581.0	7040	13889	196	751.5	4.54	0.10	2.66
	BvsC1	100	145	3.90	0.50	24.4	4959	491	12.6	1117.0	2593	4011	58.5	544.0	4.87	0.04	1.09
	C1	150	104	3.23	0.90	19.2	2608	2237	24.0	548.5	1687	4296	132	438.1	4.91	0.02	0.64
	C2	160	NA	NA	NA	NA	NA	NA	NA	NA	NA	NA	NA	NA	NA	NA	NA
	C3	180	NA	NA	NA	NA	NA	NA	NA	NA	NA	NA	NA	NA	NA	NA	NA
	C4	200	NA	NA	NA	NA	NA	NA	NA	NA	NA	NA	NA	NA	NA	NA	NA

Appendix Table 2: Particle size distribution measured by the Laboratory of K-GEO.

Profile	Soil horizon	Depth	Particle size distribution								
		(cm)	< 0.002 mm	< 0.01 mm	0.01 - 0.05 mm	0.05 - 0.1 mm	0.1 - 2.0 mm	2 - 4 mm	4 - 8 mm	8 - 16 mm	16 - 32 mm
61	Ah	5	0	1	13	12	48	10	8	5.5	2.5
	(AhBv)	15	0	1.5	17	12	49.5	8	7	3	2
	Bv	30	0	1.5	10	7.5	53	13	10	4.5	0.5
	Bv2	50	0	1.5	8	6	51.5	13	10.5	6.5	3
	BvC1	80	0	1	7	8	55	12	8.5	5.5	3
	C1	110	0	1	6.5	7.5	55	13	10	5	2
	C2	140	0	1	9	12	72	3.5	1.5	1	0
	C3	160	0	0	4	4	50	16	13	9	4
	C4	200	0	0.5	7	8	59.5	13	9	3	0
173	Ah	5	0	0	11.5	13	67	5.5	2	1	0
	E	10	1	6.5	17.5	9	40	9.5	7.5	5.5	3.5
	Bhs	14	0	1.5	15.5	11	52	9	7	4	0
	Bs	30	0	1.5	10	9	55.5	12	7	3.5	1.5
	Bs2	50	0	2	10.5	7.5	47.5	11	9.5	8	4
	BsC1	100	1.5	6.5	10	7	39	14	13	9	0
	C2	150	0.5	3	8.5	4.5	38.5	12	13	13	7

Appendix

Profile	Soil horizon	Depth (cm)	Particle size distribution								
			< 0.002 mm	< 0.01 mm	0.01 - 0.05 mm	0.05 - 0.1 mm	0.1 - 2.0 mm	2 - 4 mm	4 - 8 mm	8 - 16 mm	16 - 32 mm
177	Ah	5	0	0.5	9.5	5	67	8.5	5.5	3	1
	AhBvs	15	0	1	14.5	12.5	52	8	6	4	2
	Bvs	30	0	1	9	7	44.5	12.5	11	10	5
	Bvs2	50	0	2	8	6	44	14	12	9.5	4.5
	BvsC1	100	0	3	12	7.5	40	11.5	11	10	5
	C1	150	0	0.5	4	5	50.5	16	12	8	4
	C2	160	0	0.5	4	3	49.5	17	16	10	0
	C3	180	0	1	4	5	44	15	14	11	6
	C4	200	0	0.5	5.5	4	38	16	16	13.5	6.5

Appendix Table 3: C and N content measured in Zurich with the Piccaro and the IRMS. Additional 3 remeasured samples for particle size distribution.

Profile	Horizon	Depth	δ¹³C	C	δ¹³C	C	δ¹⁵N	N	Particle size distribution		
			Piccaro		IRMS						
		(cm)	(‰)	(%)	(‰)	(%)	(‰)	(%)	< 0.002 mm	0.002 - 0.063 mm	0.063 - 2 mm
61	Ah(Bv)	15	-25.4	1.61	-31.74	5.95	6.05	0.40			
	Bv	30	-25.9	0.66	-26.98	2.34	7.45	0.17	26	29	45
	Bv2	50	-25.7	0.35	-25.68	1.34	8.52	0.09			
	BvC1	80	-25.8	0.25	-25.54	0.94	9.07	0.07			
	C1	100	-26.1	0.17	-26.60	0.77	10.69	0.04			
	C2	140	-26.3	0.10	-25.69	0.36	11.10	0.02			
173	Ah/E	10	-25.3	1.54	-27.79	5.80	6.26	0.25			
	Bhs	14	-25.3	1.55	-29.42	5.35	9.57	0.23			
	Bs	30	-25.7	1.61	-30.41	5.44	11.02	0.18	10.6	33.1	56.3
	Bs2	50	-26.1	0.81	-26.61	3.25	11.20	0.10			
	BsC1	100	-26.6	0.08	-25.72	0.35	NA	0.02			
	C2	150	-32.4	0.00	-27.37	0.11	NA	0.00			
177	AhBvs	15	-24.8	4.56	NA	15.66	1.29	0.91			
	Bvs	30	-25.7	1.45	-26.71	4.29	7.15	0.22			
	Bvs2	50	-25.9	0.55	-26.21	1.75	7.60	0.09	4.3	23	72.7
	BvsC1	100	-27.2	0.15	-25.90	0.52	NA	0.03			
	C2	160	-33.5	-0.01	-27.80	0.09	NA	0.00			

Appendix

Appendix Table 4: XRF values measured in Zurich. AE = Abs. Error.

Profile	Horizon	Depth (cm)	Na (%)	Na AE (%)	Mg (%)	Mg AE (%)	Al (%)	Al AE (%)	Si (%)	Si AE (%)	P %	P AE (%)	K (%)	K AE (%)	Ca (%)	Ca AE (%)	Ti (%)	Ti AE (%)	Mn (%)	Mn AE (%)	Fe %	Fe AE (%)
61	Ah(Bv)	15	1.06	0.03	0.78	0.01	6.13	0.02	22.12	0.02	0.20	0	2.02	0	0.56	0	0.68	0	0.08	0	3.89	0
	Bv	30	1.18	0.04	0.93	0.01	7.68	0.02	24.99	0.03	0.13	0	2.23	0	0.63	0	0.76	0	0.12	0	4.42	0
	Bv2	50	1.13	0.04	1.00	0.01	7.99	0.02	24.23	0.03	0.11	0	2.17	0	0.63	0	0.74	0	0.12	0	4.45	0
	BvC1	80	1.18	0.04	0.95	0.01	7.82	0.02	25.58	0.03	0.09	0	2.30	0	0.69	0	0.74	0	0.08	0	4.08	0
	C1	100	1.09	0.04	1.03	0.01	8.26	0.02	25.04	0.03	0.08	0	2.37	0	0.80	0	0.75	0	0.06	0	4.40	0
	C2	140	1.34	0.04	1.27	0.02	9.70	0.02	22.13	0.03	0.10	0	2.65	0	1.03	0	0.86	0	0.06	0	5.45	0
173	Ah/E	10	0.97	0.03	0.24	0.01	4.88	0.01	31.27	0.03	0.02	0	3.07	0	0.29	0	0.48	0	0.01	0	0.73	0
	Bhs	14	0.90	0.03	0.29	0.01	5.64	0.02	27.44	0.03	0.03	0	2.72	0	0.30	0	0.53	0	0.01	0	2.45	0
	Bs	30	1.16	0.04	0.43	0.01	7.42	0.02	23.25	0.02	0.03	0	2.23	0	0.35	0	0.48	0	0.02	0	3.25	0
	Bs2	50	1.18	0.04	0.50	0.01	7.63	0.02	25.53	0.03	0.03	0	2.60	0	0.42	0	0.49	0	0.02	0	3.06	0
	BcC1	100	1.25	0.04	1.01	0.01	8.34	0.02	26.64	0.03	0.08	0	2.75	0	0.59	0	0.56	0	0.05	0	3.28	0
	C2	150	2.76	0.05	1.04	0.01	8.28	0.02	24.71	0.03	0.14	0	3.47	0	0.41	0	0.56	0	0.05	0	3.14	0
177	AhBvs	15	1.26	0.03	0.45	0.01	3.77	0.01	16.30	0.02	0.11	0	1.31	0	0.56	0	0.43	0	0.02	0	2.41	0
	Bvs	30	1.26	0.04	0.85	0.01	7.99	0.02	21.89	0.02	0.10	0	1.70	0	0.72	0	0.66	0	0.04	0	3.92	0
	Bvs2	50	1.23	0.04	1.09	0.01	8.65	0.02	22.79	0.02	0.13	0	2.00	0	0.79	0	0.68	0	0.04	0	3.98	0
	BvsC1	100	1.46	0.04	1.50	0.02	8.95	0.02	22.48	0.02	0.12	0	2.42	0	1.06	0	0.84	0	0.05	0	4.69	0
	C2	160	1.96	0.05	1.56	0.02	8.71	0.02	22.26	0.02	0.15	0	2.56	0	1.90	0	0.92	0	0.06	0	5.24	0

Appendix Table 5: Values for meteoric ^{10}Be measurement.

Profile	Horizon	Depth (cm)	Thickness (cm)	Density (g/cm²)	Weight (g/cm²)	^{10}Be atoms per g (1E8)	Error (%)	Error (^{10}Be atoms per g) (1E8)	Skeleton content (%)
61	Ah(Bv)	15	15	0.71	10.58	2.77	2.00	0.00	26
	Bv	30	15	0.79	11.91	5.16	2.00	0.10	28
	Bv2	50	20	0.85	16.92	5.78	2.00	0.12	33
	BvC1	80	30	0.98	29.34	3.74	2.00	0.07	29
	C1	100	20	1.08	21.66	6.25	2.00	0.13	30
	C2	140	40	1.04	41.40	4.04	2.00	0.08	30
173	Ah/E	10	10	0.81	8.10	0.28	2.36	0.01	9
	Bhs	14	4	0.58	2.32	0.63	2.02	0.01	26
	Bs	30	16	0.67	10.64	3.75	2.00	0.08	24
	Bs2	50	20	0.80	15.92	3.87	2.00	0.08	33
	BsC1	100	50	1.46	73.10	2.81	2.00	0.06	36
	C2	150	50	1.36	68.15	0.83	2.02	0.02	45
177	AhBvs	15	15	0.63	9.44	1.26	2.01	0.03	19
	Bvs	30	15	0.71	10.64	6.53	2.00	0.13	39
	Bvs + BcsC1	50	70	0.85	59.43	4.57	2.00	0.09	39
	C2	100	60	1.30	77.70	0.29	2.26	0.01	42

Appendix

Appendix Table 6: Values for in situ ^{10}Be measurement.

Profile	Description	Latitude (°)	Longitude (°)	Elevation (m a.s.l.)	Shielding factor	Sample thickness (cm)	Rock density (g/cm²)	^{10}Be (atmos/g x 10^4)	Exposure age (year)
61	Rock Hill Height 10	48.67	14.71	730	0.622	2.0	2.65	11.35	22301
	Rock Hill Height 110	48.67	14.71	730	0.869	2.0	2.65	24.08	35648
	Rock Hill Height 180	48.67	14.71	730	0.714	2.0	2.65	35.63	66695
177	Tree uproot 1	48.66	14.71	745	0.499	2.0	2.65	16.74	42063
	Tree uproot 2	48.66	14.71	745	0.671	2.0	2.65	16.15	30091
	Belowground Depth 35cm	48.66	14.71	736	0.993	1.5	2.65	16.89	21348
	Tree uproot 3	48.66	14.71	728	0.983	1.5	2.65	24.55	32013
	Tree uproot 4	48.66	14.71	728	0.995	1.0	2.65	26.82	34524

Appendix Table 7: Values for Pu measurement of profile 61.

Profile	Site	Description	Density (g/cm³)	$^{239+240}$Pu activity (Bq/kg)	Site	Description	Density (g/cm³)	$^{239+240}$Pu activity (Bq/kg)	Site	Description	Density (g/cm³)	$^{239+240}$Pu activity (Bq/kg)
61	Reference	R1.1	0.51	4.349	Erosion	E1.1	0.66	1.648	TUR	T1.1	0.86	1.482
		R1.2	0.74	0.243		E1.2	0.75	0.640		T1.2	0.80	0.021
		R1.3	0.64	0.051		E1.3	0.53	0.190		T1.3	0.75	0.022
		R1.4	0.71	0.081		E1.4	0.75	0.104		T1.4	0.66	0.007
		R2.1	0.66	1.515		E2.1	0.66	0.633		T2.1	0.65	1.870
		R2.2	0.62	0.320		E2.2	0.59	0.308		T2.2	0.67	0.525
		R2.3	0.62	0.198		E2.3	0.53	0.077		T2.3	0.77	0.041
		R2.4	0.69	0.017		E2.4	0.68	0.046		T2.4	0.86	0.014
		R3.1	0.74	1.363		E3.1	0.43	1.969		T3.1	0.77	0.531
		R3.2	0.74	0.099		E3.2	0.56	0.087		T3.2	0.69	0.022
		R3.3	0.66	0.241		E3.3	0.76	0.013		T3.3	0.69	0.005
		R3.4	0.73	0.009		E3.4	0.84	0.008		T3.4	0.74	0.011
		R4.1	0.70	1.315		E4.1	0.69	1.489		T4.1	0.68	1.778
		R4.2	0.69	0.106		E4.2	0.51	0.560		T4.2	0.68	0.043
		R4.3	0.72	0.080		E4.3	0.39	0.254		T4.3	0.69	0.022
		R4.4	0.77	0.005		E4.4	0.68	0.051		T4.4	0.71	0.032

Appendix

Appendix Table 8: Values for Pu measurement of profile 173.

Profile	Site	Description	Density (g/cm³)	$^{239+240}$Pu activity (Bq/kg)	Site	Description	Density (g/cm³)	$^{239+240}$Pu activity (Bq/kg)
173	Reference	R1.1	0.41	0.496	Erosion	E1.1	0.16	2.594
		R1.2	0.49	0.128		E1.2	0.26	0.310
		R1.3	0.53	0.043		E1.3	0.57	0.095
		R1.4	0.65	0.013		E1.4	0.51	0.167
		R2.1	0.59	1.797		E2.1	0.26	3.519
		R2.2	0.49	0.439		E2.2	0.54	0.289
		R2.3	0.52	0.151		E2.3	0.46	0.219
		R2.4	0.59	0.035		E2.4	0.42	0.041
		R3.1	0.46	1.955		E3.1	0.15	0.716
		R3.2	0.60	0.251		E3.2	0.52	0.188
		R3.3	0.55	0.057		E3.3	0.41	0.389
		R3.4	0.59	0.024		E3.4	0.55	0.102
		R4.1	0.45	1.662		E4.1	0.14	0.696
		R4.2	0.57	0.306		E4.2	0.41	1.006
		R4.3	0.64	0.049		E4.3	0.46	0.574
		R4.4	0.57	0.032		E4.4	0.38	0.117

Appendix Table 9: Values for Pu measurement of profile 177.

Profile	Site	Description	Density (g/cm³)	$^{239+240}$Pu activity (Bq/kg)	Site	Description	Density (g/cm³)	$^{239+240}$Pu activity (Bq/kg)
177	Reference	R1.1	0.54	1.168	Erosion	E1.1	0.32	2.453
		R1.2	0.75	0.054		E1.2	0.50	0.459
		R1.3	0.67	0.093		E1.3	0.51	0.069
		R1.4	0.76	0.023		E1.4	0.51	0.044
		R2.1	0.59	1.533		E2.1	0.53	2.382
		R2.2	0.65	0.098		E2.2	0.53	0.228
		R2.3	0.69	0.012		E2.3	0.53	0.048
		R2.4	0.78	0.003		E2.4	0.50	0.018
		R3.1	0.62	0.704		E3.1	0.26	1.542
		R3.2	0.69	0.056		E3.2	0.52	0.219
		R3.3	0.72	0.037		E3.3	0.55	0.131
		R3.4	0.64	0.010		E3.4	0.56	0.140
		R4.1	0.63	0.873		E4.1	0.40	2.953
		R4.2	0.66	0.048		E4.2	0.51	0.103
		R4.3	0.72	0.042		E4.3	0.53	0.040
		R4.4	0.72	0.018		E4.4	0.48	0.100

Appendix

Appendix Table 10: Values after wet and dry sieving for aggregate stability. OM = Organic Matter.

Profile	Aggregate	Particle size distribution										
		Dry sieving				Wet sieving						
		Total used material	> 5 mm	> 2 mm	< 2 mm	Total used material	OM	> 1 mm	> 500 µm	> 250 µm	> 125 µm	< 125 µm
		(g)	(g)	(g)	(g)	(g)	(g)	(g)	(g)	(g)	(g)	(g)
61	1	103.20	48.80	28.80	25.40	20.30	1.20	10.80	5.00	1.20	0.70	0.50
	2	86.10	34.80	26.40	24.50	20.20	0.50	10.60	5.40	1.60	0.70	0.60
	3	98.10	51.00	24.00	22.90	18.50	2.60	8.70	3.70	1.70	0.80	0.40
	4	125.40	22.80	40.30	61.80	24.00	1.00	10.30	6.70	2.50	1.50	1.30
173	1	43.00	6.30	12.50	24.10	18.90	2.60	6.60	5.00	2.30	0.80	0.80
	2	91.10	36.70	26.90	27.10	20.10	4.80	8.10	2.40	2.00	1.30	1.00
	3	68.70	19.70	20.50	28.30	21.00	3.20	8.60	4.00	2.90	0.90	0.60
	4	50.20	12.10	14.60	23.30	18.10	3.80	6.60	4.40	1.70	0.70	0.50
177	1	215.70	58.00	72.20	84.10	84.10	6.50	21.90	14.90	16.40	9.00	6.70
	2	195.00	41.60	47.20	94.30	10.20	1.20	8.00	0.10	0.10	0.06	0.04
	3	114.90	25.50	35.30	53.60	20.20	3.60	7.90	3.70	2.10	1.20	0.90
	4	161.20	39.40	51.50	69.70	22.00	4.30	10.30	2.70	2.40	0.90	0.60

Personal Declaration

I hereby declare that the submitted thesis is the result of my own, independent work. All external sources are explicitly acknowledged in the thesis.

_____

Teresa Steinert

Zürich, 14.07.2018

Acknowledgements

I would like to thank several people for helping and guiding me through my master thesis.

First of all, I would like to thank my main supervisor Prof. Dr. Markus Egli. He helped me through my entire time. Starting with the field work and going through the lab measurement with all the barriers we had to go through. Additionally, he helped me with understanding the broader context of the topic and supported me with calculations and several helpful discussions.

I would also thank Samuel Abiven supporting me with discussions and critical feedback. He kindly supports me with R coding, that would be much harder without him.

Pavel Danek and Pavel Samonil helped me generously in the field, especially carrying the heavy samples and refilling the soil profiles. Thanks to Pavel Samonil that I could be part of this research project. He provided previous soil analysis, and we had an intensive discussion about the results.

I own a big thank to the whole lab group helping me with the lab procedures, explanation of the equipment and general support of my master thesis. Namely, I want to thank Dr. Dagmar Brandová, helping me through the entire ^{10}Be measurements. Raquel de Castro, for guiding me through the Pu measurements. Alessandra Musso, for analysing the Pu in my samples. Thomy Keller and Tatjana Kraut, for analysing the C and N content in my samples. And last but not least Francesca Calitri helping me a lot with equations and understanding principles of Pu.

Finally, I would like to thank my family and best friends for their support in their own best possible way. They helped me in several working or personal processes and helped me to focus on the main challenges. My brother owns special thanks for taking his time proof-reading and giving constructive feedback even though he is not from the topic.